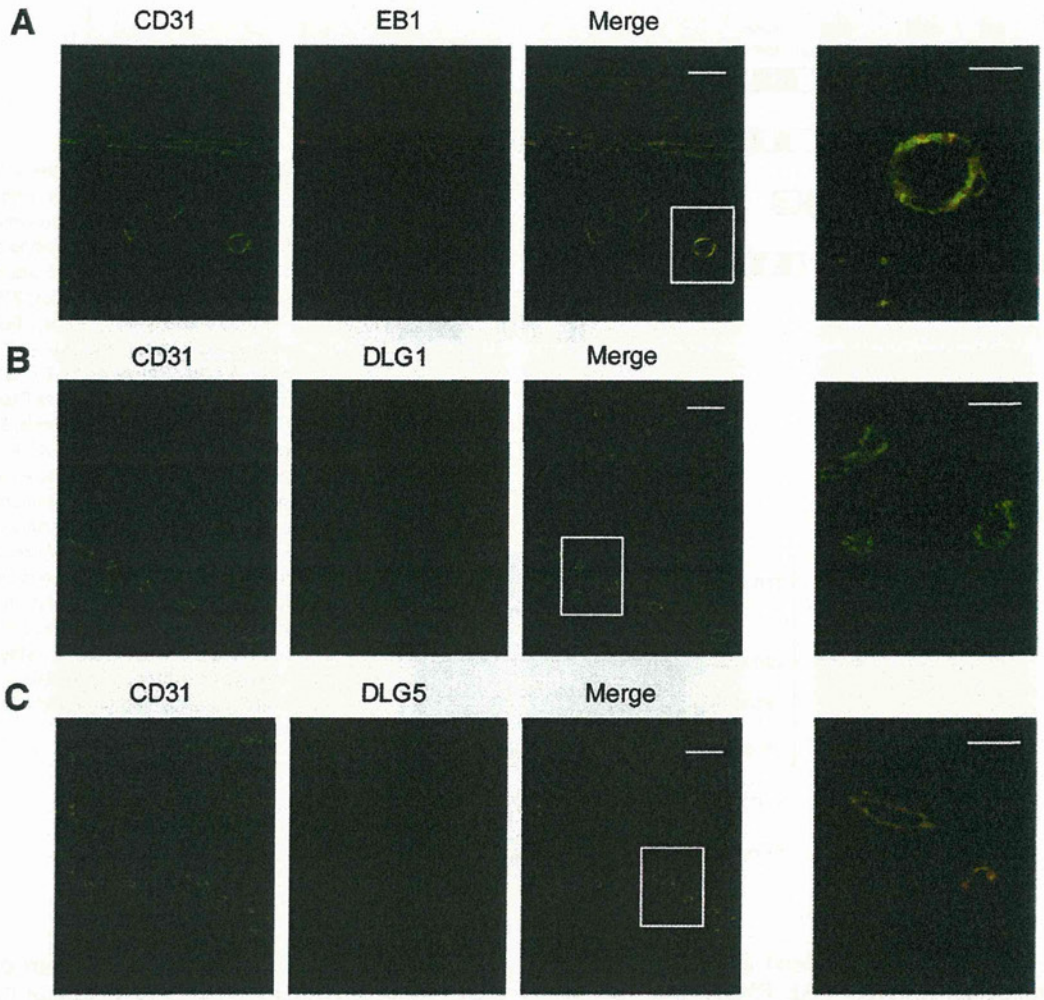

Figure 7 Localization of EB1 and DLG5 in the vascular endothelial cells of inflamed colon of F344 rats. Representative images of CD31 and EB1 (**A**), DLG1 (**B**) or DLG5 (**C**) co-fluorescent staining of distal colonic lesions from F344 rats immediately after DSS treatment (week 1). EB1 and DLG5, but not DLG1, were highly expressed in VECs at the submucosa. Scale bar = 50 μm. Images in the **right column** are magnified from the **boxed areas** of the merged images. Scale bar = 20 μm.

Fluorescent IHC analysis of inflamed colonic tissue at week 1, immediately after DSS treatment, revealed that EB1 and DLG5, but not DLG1, were expressed in the VECs (Figure 7). EB1 was also expressed in the severely ulcerated mucosal region (Figure 7A). DLG1, DLG5, and EB1 were not expressed in the VECs of the colon before the DSS treatment (data not shown). Thus, these findings indicate that the expression of EB1 and DLG5 was induced in VECs when colon inflammation occurred and that DLG5, rather than EB1, showed a pattern of expression similar to that of the APC protein (Figure 3).

Discussion

APC has been identified as the causative gene of the familial adenomatous polyposis of the colon. APC negatively regulates Wnt signaling by interacting with β-catenin via its β-catenin binding sites. Truncation of the APC protein at β-catenin binding sites result in the activation of Wnt signaling, which is a hallmark of the initiation of carcinogenesis in colonic epithelial cells.[12,28,29] In KAD rats (homozygous for the $Apc^{\Delta 2523}$ mutation), Wnt signaling is normal because the β-catenin binding sites are intact. Thus, we could exclude the effects of Wnt signaling when we compared physiologic characteristics found in KAD and control F344 rats. Alternatively, we could ascribe characteristic differences to the physiologic function of the C terminus of APC.

Even 3 weeks after terminating DSS treatment, KAD rats had continuous elevation of the expression of inflammatory-related genes, such as *Cox2* and *Ptges*, and enhanced cell proliferation, which were coincident with persistent inflammation. COX-2 and PTGES are functionally coupled for the biosynthesis of prostaglandin E2,[30] which plays a critical role during tumorigenesis in the gastrointestinal tract.[31,32] Thus, these findings can explain the significantly

higher incidences and multiplicities of colon tumors found in KAD rats compared with the control F344 rats.[16]

Immediately after DSS treatment, KAD rats had an abnormal deposition of fibrin in microvessels, instead of a normal formation of fibrin layers to cover the damaged mucosa. KAD rats also had decreased microvessel angiogenesis in the damaged colonic mucosa immediately after DSS treatment. Given the evident increase in expression of APC in VECs of the edematous submucosa, it is likely that APC has a critical role in angiogenesis that is driven in response to acute inflammation of the colon and that KAD rats have defects in such angiogenesis. Such defects may result in a delay in the repair process of the damaged mucosa possibly because of the shortage of oxygen and nutrition supply and therefore a persistence of colitis in KAD rats.

To determine how APC is involved in angiogenesis, we characterized the physiologic function of VECs of KAD rats. KAD rat VECs had stronger adhesion and formed abnormal tube morphology, which was characterized by a smaller number of branching points and a shorter length when VECs were stimulated to form tubes on Matrigel. The adhesion activity of VECs plays an important role in tube formation.[33,34] Therefore, it is likely that the enhanced adhesion activity may result in the low branched and short tubes found in KAD rat VECs. Although VECs were prepared from the thoracic aorta in this study, defects in tube formation may explain the decreased number of microvessels found in the damaged colonic mucosa of KAD rats.

Expression of both APC and DLG5 was specifically induced in the VEC of the inflamed colon at week 1, immediately after DSS treatment. DLG5 interacted with the C terminus of APC, probably via its PDZ domains. The DLG protein family interacts with transmembrane proteins in endothelial cells and is associated with angiogenesis.[35] Thus, we consider that the APC-DLG5 molecular pathway may function in the regulation of angiogenesis and cell adhesion of VECs.

It is known that abnormal angiogenesis contributes to the initiation and perpetuation of IBD and that microvessel dysfunction causes poor mucosal healing in IBD.[36,37] Similar to IBD patients, KAD rats had reduced angiogenesis in the inflamed mucosa and the KAD VECs had reduced adhesion activity. The human *DLG5* locus is associated with the pathogenesis of IBD.[27] In rats, expression of DLG5 can be induced by DSS treatment, and DLG5 binds to the C terminus of APC, which is absent in KAD rats. These results suggest that both APC and DLG5 may be involved in the pathogenesis of IBD. Further genetic analysis of relevant human populations may clarify the involvement of APC in the development of colitis.

It is expected that mutant APC derived from the $Apc^{\Delta 2523}$ allele may coexist with wild-type APC in the heterozygous KAD ($Apc^{\Delta 2523}/+$) rat because transcripts from the mutant allele can escape nonsense-mediated decay. Thus, further study using heterozygous rats may reveal dominant negative functions of the mutant APC.

In summary, we found a new function of APC in the pathogenesis of colonic inflammation, which appears to be mediated by the regulation of cellular adhesion activity of VECs. Molecular interaction of APC with DLG5 may function in the regulation of angiogenesis and cell adhesion of VECs. Our findings suggest that APC may contribute to the pathogenesis of IBD, in which patients are more susceptible to colorectal cancers.

Acknowledgments

We thank Dr. Hiroshi Hiai for his critical reading of the manuscript.

Supplemental Data

Supplemental material for this manuscript can be found at *http://dx.doi.org/10.1016/j.ajpath.2012.12.005*.

References

1. Wallace JL, Vong L, Dharmani P, Srivastava V, Chadee K: Muc-2-deficient mice display a sex-specific: COX-2-related impairment of gastric mucosal repair. Am J Pathol 2011, 178:1126–1133
2. Tonnesen MG, Feng X, Clark RA: Angiogenesis in wound healing. J Investig Dermatol Symp Proc 2000, 5:40–46
3. Tarnawski AS: Cellular and molecular mechanisms of gastrointestinal ulcer healing. Dig Dis Sci 2005, 50(Suppl 1):S24–S33
4. Podolsky DK: Inflammatory bowel disease. N Engl J Med 2002, 347: 417–429
5. Bernstein CN, Blanchard JF, Kliewer E, Wajda A: Cancer risk in patients with inflammatory bowel disease: a population-based study. Cancer 2001, 91:854–862
6. Danese S, Sans M, Fiocchi C: Inflammatory bowel disease: the role of environmental factors. Autoimmun Rev 2004, 3:394–400
7. Cooney R, Jewell D: The genetic basis of inflammatory bowel disease. Dig Dis 2009, 27:428–442
8. Kawada M, Arihiro A, Mizoguchi E: Insights from advances in research of chemically induced experimental models of human inflammatory bowel disease. World J Gastroenterol 2007, 13: 5581–5593
9. Okayasu I, Hatakeyama S, Yamada M, Ohkusa T, Inagaki Y, Nakaya R: A novel method in the induction of reliable experimental acute and chronic ulcerative colitis in mice. Gastroenterology 1990, 98: 694–702
10. Groden J, Thliveris A, Samowitz W, Carlson M, Gelbert L, Albertsen H, Joslyn G, Stevens J, Spirio L, Robertson M, Sargeant L, Krapcho K, Wolff E, Burt R, Hughes JP, Warrington J, McPherson J, Wasmuth J, Le Paslier D, Abderrahim H, Cohen D, Leppert M, White R: Identification and characterization of the familial adenomatous polyposis coli gene. Cell 1991, 66:589–600
11. Oshima M, Oshima H, Kitagawa K, Kobayashi M, Itakura C, Taketo M: Loss of Apc heterozygosity and abnormal tissue building in nascent intestinal polyps in mice carrying a truncated Apc gene. Proc Natl Acad Sci U S A 1995, 92:4482–4486
12. Aoki K, Taketo MM: Adenomatous polyposis coli (APC): a multifunctional tumor suppressor gene. J Cell Sci 2007, 120:3327–3335
13. Beroud C, Soussi T: APC gene: database of germline and somatic mutations in human tumors and cell lines. Nucleic Acids Res 1996, 24: 121–124
14. Smits R, Kielman MF, Breukel C, Zurcher C, Neufeld K, Jagmohan-Changur S, Hofland N, van Dijk J, White R, Edelmann W,

Kucherlapati R, Khan PM, Fodde R: Apc1638T: a mouse model delineating critical domains of the adenomatous polyposis coli protein involved in tumorigenesis and development. Genes Dev 1999, 13: 1309–1321
15. Yokoyama A, Nomura R, Kurosumi M, Shimomura A, Onouchi T, Iizuka-Kogo A, Smits R, Oda N, Fodde R, Itoh M, Senda T: The C-terminal domain of the adenomatous polyposis coli (Apc) protein is involved in thyroid morphogenesis and function. Med Mol Morphol 2011, 44:207–212
16. Yoshimi K, Tanaka T, Takizawa A, Kato M, Hirabayashi M, Mashimo T, Serikawa T, Kuramoto T: Enhanced colitis-associated colon carcinogenesis in a novel Apc mutant rat. Cancer Sci 2009, 100:2022–2027
17. Yoshimi K, Hashimoto T, Niwa Y, Hata K, Serikawa T, Tanaka T, Kuramoto T: Use of a chemically induced-colon carcinogenesis-prone Apc-mutant rat in a chemotherapeutic bioassay. BMC Cancer 2012, 12:448
18. Melgar S, Karlsson A, Michaelsson E: Acute colitis induced by dextran sulfate sodium progresses to chronicity in C57BL/6 but not in BALB/c mice: correlation between symptoms and inflammation. Am J Physiol Gastrointest Liver Physiol 2005, 288:G1328–G1338
19. Vermeulen PB, Gasparini G, Fox SB, Toi M, Martin L, McCulloch P, Pezzella F, Viale G, Weidner N, Harris AL, Dirix LY: Quantification of angiogenesis in solid human tumours: an international consensus on the methodology and criteria of evaluation. Eur J Cancer 1996, 32A: 2474–2484
20. Feroze-Merzoug F, Berquin IM, Dey J, Chen YQ: Peptidylprolyl isomerase A (PPIA) as a preferred internal control over GAPDH and beta-actin in quantitative RNA analyses. Biotechniques 2002, 32: 776–778, 780, 782
21. Shi W, Wang NJ, Shih DM, Sun VZ, Wang X, Lusis AJ: Determinants of atherosclerosis susceptibility in the C3H and C57BL/6 mouse model: evidence for involvement of endothelial cells but not blood cells or cholesterol metabolism. Circ Res 2000, 86:1078–1084
22. Kroboth K, Newton IP, Kita K, Dikovskaya D, Zumbrunn J, Waterman-Storer CM, Nathke IS: Lack of adenomatous polyposis coli protein correlates with a decrease in cell migration and overall changes in microtubule stability. Mol Biol Cell 2007, 18:910–918
23. Matsumoto S, Fumoto K, Okamoto T, Kaibuchi K, Kikuchi A: Binding of APC and dishevelled mediates Wnt5a-regulated focal adhesion dynamics in migrating cells. EMBO J 2010, 29:1192–1204
24. Shimizu T, Suzuki M, Fujimura J, Hisada K, Yoshikazu O, Obinata K, Yamashiro Y: The relationship between the concentration of dextran sodium sulfate and the degree of induced experimental colitis in weanling rats. J Pediatr Gastroenterol Nutr 2003, 37:481–486
25. Ingber DE: Mechanical signaling and the cellular response to extracellular matrix in angiogenesis and cardiovascular physiology. Circ Res 2002, 91:877–887
26. Li D, Xie S, Ren Y, Huo L, Gao J, Cui D, Liu M, Zhou J: Microtubule-associated deacetylase HDAC6 promotes angiogenesis by regulating cell migration in an EB1-dependent manner. Protein Cell 2011, 2: 150–160
27. McGovern DP, Gardet A, Torkvist L, Goyette P, Essers J, Taylor KD, Neale BM, Ong RT, Lagace C, Li C, Green T, Stevens CR, Beauchamp C, Fleshner PR, Carlson M, D'Amato M, Halfvarson J, Hibberd ML, Lordal M, Padyukov L, Andriulli A, Colombo E, Latiano A, Palmieri O, Bernard EJ, Deslandres C, Hommes DW, de Jong DJ, Stokkers PC, Weersma RK, Sharma Y, Silverberg MS, Cho JH, Wu J, Roeder K, Brant SR, Schumm LP, Duerr RH, Dubinsky MC, Glazer NL, Haritunians T, Ippoliti A, Melmed GY, Siscovick DS, Vasiliauskas EA, Targan SR, Annese V, Wijmenga C, Pettersson S, Rotter JI, Xavier RJ, Daly MJ, Rioux JD, Seielstad M: Genome-wide association identifies multiple ulcerative colitis susceptibility loci. Nat Genet 2010, 42:332–337
28. Akiyama T, Kawasaki Y: Wnt signalling and the actin cytoskeleton. Oncogene 2006, 25:7538–7544
29. Senda T, Iizuka-Kogo A, Onouchi T, Shimomura A: Adenomatous polyposis coli (APC) plays multiple roles in the intestinal and colorectal epithelia. Med Mol Morphol 2007, 40:68–81
30. Murakami M, Naraba H, Tanioka T, Semmyo N, Nakatani Y, Kojima F, Ikeda T, Fueki M, Ueno A, Oh S, Kudo I: Regulation of prostaglandin E2 biosynthesis by inducible membrane-associated prostaglandin E2 synthase that acts in concert with cyclooxygenase-2. J Biol Chem 2000, 275:32783–32792
31. Oshima M, Dinchuk JE, Kargman SL, Oshima H, Hancock B, Kwong E, Trzaskos JM, Evans JF, Taketo MM: Suppression of intestinal polyposis in $Apc^{\Delta 716}$ knockout mice by inhibition of cyclooxygenase 2 (COX-2). Cell 1996, 87:803–809
32. Sonoshita M, Takaku K, Sasaki N, Sugimoto Y, Ushikubi F, Narumiya S, Oshima M, Taketo MM: Acceleration of intestinal polyposis through prostaglandin receptor EP2 in $Apc^{\Delta 716}$ knockout mice. Nat Med 2001, 7:1048–1051
33. Drake CJ, Hungerford JE, Little CD: Morphogenesis of the first blood vessels. Ann N Y Acad Sci 1998, 857:155–179
34. Davis GE, Stratman AN, Sacharidou A, Koh W: Molecular basis for endothelial lumen formation and tubulogenesis during vasculogenesis and angiogenic sprouting. Int Rev Cell Mol Biol 2011, 288: 101–165
35. Yamamoto Y, Irie K, Asada M, Mino A, Mandai K, Takai Y: Direct binding of the human homologue of the Drosophila disc large tumor suppressor gene to seven-pass transmembrane proteins, tumor endothelial marker 5 (TEM5), and a novel TEM5-like protein. Oncogene 2004, 23:3889–3897
36. Koutroubakis IE, Tsiolakidou G, Karmiris K, Kouroumalis EA: Role of angiogenesis in inflammatory bowel disease. Inflamm Bowel Dis 2006, 12:515–523
37. Papa A, Scaldaferri F, Danese S, Guglielmo S, Roberto I, Bonizzi M, Mocci G, Felice C, Ricci C, Andrisani G, Fedeli G, Gasbarrini G, Gasbarrini A: Vascular involvement in inflammatory bowel disease: pathogenesis and clinical aspects. Dig Dis 2008, 26:149–155

Transcription factors c-Myc and CDX2 mediate E-selectin ligand expression in colon cancer cells undergoing EGF/bFGF-induced epithelial–mesenchymal transition

Keiichiro Sakuma[a], Masahiro Aoki[a], and Reiji Kannagi[a,b,c,1]

[a]Division of Molecular Pathology, Aichi Cancer Center, Chikusa-ku, Nagoya, Aichi 464-8681, Japan; [b]Research Complex for Medical Frontiers, Aichi Medical University, Yazako, Nagakute, Aichi 480-1195, Japan; and [c]Institute of Biomedical Sciences, Academia Sinica, Taipei 115, Taiwan

Edited* by Sen-itiroh Hakomori, Pacific Northwest Research Institute, Seattle, WA, and approved April 5, 2012 (received for review July 11, 2011)

Sialyl Lewis x (sLe^x) and sialyl Lewis a (sLe^a) glycans are expressed on highly metastatic colon cancer cells. They promote extravasation of cancer cells and tumor angiogenesis via interacting with E-selectin on endothelial cells. Recently, epithelial–mesenchymal transition (EMT) has been noted as a critical phenotypic alteration in metastatic cancer cells. To address the association between $sLe^{x/a}$ expression and EMT, we assessed whether $sLe^{x/a}$ are highly expressed on colon cancer cells undergoing EMT. Treatment of HT29 and DLD-1 cells with EGF and/or basic FGF (bFGF) induced EMT and significantly increased $sLe^{x/a}$ expression resulting in enhanced E-selectin binding activity. The transcript levels of the glycosyltransferase genes *ST3GAL1/3/4* and *FUT3* were significantly elevated and that of *FUT2* was significantly suppressed by the treatment. We provide evidence that *ST3GAL1/3/4* and *FUT3* are transcriptionally up-regulated by c-Myc with probable involvement of Ser62 phosphorylation, and that *FUT2* is transcriptionally down-regulated through the attenuation of CDX2. The contribution of c-Myc and CDX2 to the $sLe^{x/a}$ induction was proved to be significant by knockdown or forced expression experiments. Interestingly, the cells undergoing EMT exhibited significantly increased VEGF secretion, which can promote tumor angiogenesis in cooperation with $sLe^{x/a}$. Finally, immunohistological study indicated high E-selectin ligand expression on cancer cells undergoing EMT in vivo, supporting their coexistence observed in vitro. These results suggest a significant link between $sLe^{x/a}$ expression and EMT in colon cancer cells and a pivotal role of c-Myc and CDX2 in regulating $sLe^{x/a}$ expression during EMT.

Colon cancer is one of the most prevalent cancers worldwide, with more than 1,200,000 new cases and over 600,000 deaths estimated to have occurred in 2008 (1). Although early detection, increased awareness, and developments in treatment have increased complete cure rates especially in some advanced countries, distant metastasis is still a critical event that makes colon cancer a lethal disease. Therefore, novel therapeutic approaches to inhibit metastasis are required.

Sialyl Lewis x (sLe^x) and sialyl Lewis a (sLe^a) are E-selectin ligand glycans expressed on the surface of many types of cancer cells, including colorectal, pancreatic, gastric, breast, prostate, and lung cancer (2, 3). These glycans play crucial roles in hematogenous metastasis through interaction with endothelial cells. The most established role is promoting extravasation of cancer cells: circulating cancer cells in blood flow arrest at distant sites by adhering to endothelial cells, which enables their movement out of the vasculature (2, 3). Importantly, the interaction between $sLe^{x/a}$ and E-selectin exclusively mediates the adhesion of most epithelial cancer cells to endothelial cells, whereas $sLe^{x/a}$-independent interaction with endothelial ICAM-1 and VCAM-1 mediates the adhesion of nonepithelial malignant cells, such as leukemia and some sarcoma cells, to endothelial cells (4). Another important role of $sLe^{x/a}$ in hematogenous metastasis is tumor angiogenesis (3, 5), which can facilitate intravasation and postextravasational proliferation of cancer cells (6–8). In line with these observations, high $sLe^{x/a}$ expression levels in colon cancer patients are correlated with poor prognosis (2). Therefore, these glycans are frequently evaluated as tumor markers. Whereas the diagnostic utility of $sLe^{x/a}$ has been well established, therapeutic approaches targeting these glycans are not well developed, partly because molecular mechanisms of their expression have been only partially elucidated (9–11).

Recently, epithelial–mesenchymal transition (EMT) has been noted as a critical event in the early step of cancer metastasis (12, 13). It is also notable that EMT is known to be associated with cancer stem cells (14, 15). EMT is defined as a transitional process from epithelial to mesenchymal phenotype, including fibroblast-like morphology, down-regulation of *E-cadherin* by transcriptional repressors such as SNAIL1, ZEB1, and TWIST, mesenchymal marker expression such as Vimentin, Fibronectin, and N-cadherin, and enhanced cell motility. A variety of EMT inducers have been reported, including TGF-β and receptor tyrosine kinase (RTK) growth factors such as hepatocyte growth factor (HGF), EGF, and basic FGF (bFGF). Although many studies have focused on TGF-β (16), the TGF-β signaling pathway is frequently inactivated in colon cancer due to loss-of-function mutations in TGFBR2 and SMAD genes (17). Therefore, RTK growth factors are likely to figure more heavily than TGF-β in EMT of colon cancer cells. Several clinical studies have suggested the correlation between RTK signaling and metastasis. EGFR was expressed in ~85% of patients with metastatic colon cancer (18) and its expression level and function in colon cancer cells were correlated with metastatic potential (19, 20). Plasma bFGF levels were significantly higher in patients with metastatic colon cancer than in normal controls, whereas those levels were comparable between patients with nonmetastatic colon cancer and normal controls (21). Sato et al. demonstrated by quantitative RT-PCR that the transcript levels of *FGFR1* in colon cancer tissues were significantly higher in patients with liver metastasis than in those without liver metastasis (22).

Despite the significant roles of $sLe^{x/a}$ and EMT in cancer metastasis, their association remains unknown. To address this issue, we assessed whether $sLe^{x/a}$ is highly expressed on cancer cells undergoing EMT.

Results

Induction of EMT in Colon Cancer Cells by EGF or bFGF. To prepare colon cancer cells undergoing EMT, we treated HT29 and DLD-1 cells with EGF (20 ng/mL) and/or bFGF (10 ng/mL) in serum-deprived medium. Treatment with either EGF or bFGF alone transiently induced a fibroblast-like appearance (Fig. 1*A*); however, it was very difficult to maintain the cells for further experiments. Treatment with both EGF and bFGF (hereafter EGF/bFGF treatment) permitted better cell survival and induced a fibroblast-

Author contributions: K.S., M.A., and R.K. designed research; K.S. performed research; K.S., M.A., and R.K. analyzed data; and K.S., M.A., and R.K. wrote the paper.

The authors declare no conflict of interest.

*This Direct Submission article had a prearranged editor.

[1]To whom correspondence should be addressed. E-mail: kannagi-gi@umin.ac.jp.

This article contains supporting information online at www.pnas.org/lookup/suppl/doi:10.1073/pnas.1111135109/-/DCSupplemental.

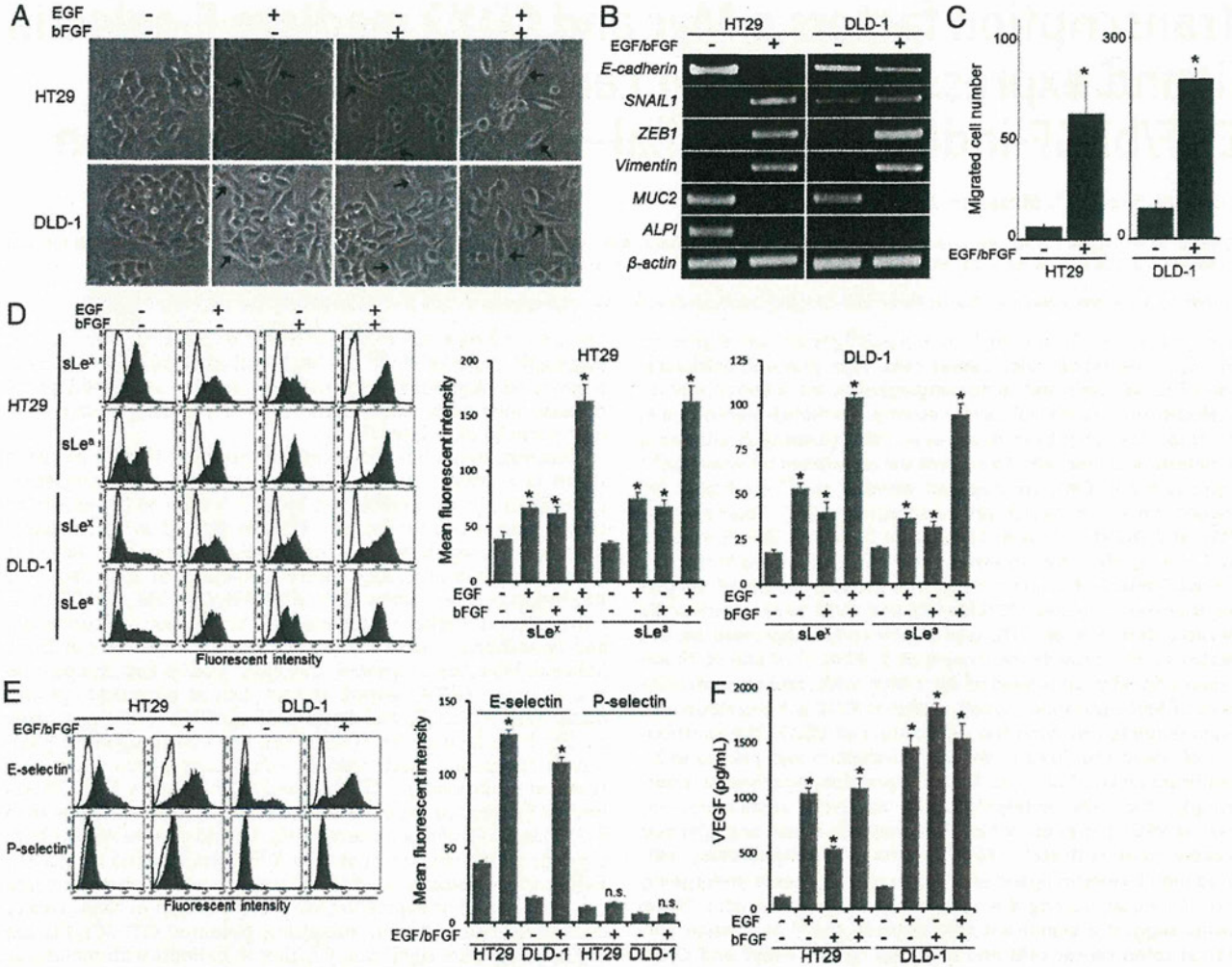

Fig. 1. Induction of EMT and sLe$^{x/a}$ expression in colon cancer cells by EGF or bFGF. (*A*) HT29 and DLD-1 cells were maintained in culture medium with 10% FBS or in serum-free medium supplemented with EGF (20 ng/mL) and/or bFGF (10 ng/mL). After culture for 7 d, cells were observed under a phase-contrast microscope. (Arrows) Cells exhibiting fibroblastic morphology. (*B*) Expression of marker genes for EMT and colon-epithelial differentiation was examined by conventional RT-PCR. (*C*) Cell migration activity was determined with Biocoat Matrigel invasion chambers. (*D*) Expression levels of sLe$^{x/a}$ were determined by flow cytometry. Bold lines, staining control. (*E*) Selectin-binding activity was determined by flow cytometry. Bold lines, staining control. (*F*) Culture supernatant VEGF levels were measured by ELISA. (*C–F*) Statistic analysis was performed in three independent experiments by *t* test. Error bars, SD; asterisks, $P < 0.05$ (*C*), $P < 0.01$ (*D*), $P < 0.000005$ (*E*), and $P < 0.0001$ (*F*) compared with the untreated cells; NS, not significant ($P > 0.05$).

like appearance (Fig. 1*A*). The EGF/bFGF treatment increased the levels of the mesenchymal marker genes *SNAIL1*, *ZEB1*, and *Vimentin*, whereas it reduced the level of *E-cadherin* and the colon-epithelial differentiation marker genes *MUC2* (mucin 2) and *ALPI* (intestinal alkaline phosphatase) (Fig. 1*B*). Functionally, the treated cells showed significantly enhanced migration activity ($P < 0.05$; Fig. 1*C*). These results indicated that the EGF/bFGF treatment induced EMT in HT29 and DLD-1 cells.

Induction of sLe$^{x/a}$ Expression and E-Selectin Binding Activity in Colon Cancer Cells by EGF or bFGF. We then evaluated sLe$^{x/a}$ expression levels on the cells undergoing EMT by flow cytometry. The results indicated significantly increased sLe$^{x/a}$ expression on the EGF/bFGF-treated cells as well as on the cells treated with either factor alone compared with the untreated cells ($P < 0.01$; Fig. 1*D*). To test whether the increased sLe$^{x/a}$ expression could contribute to the interaction with E-selectin, we examined binding activity of the treated cells to recombinant E-selectin. The cells exhibited significantly enhanced E-selectin binding activity ($P < 0.000005$), whereas no significant binding activity was detected for P-selectin ($P > 0.05$; Fig. 1*E*), which selectively binds to sLe^x determinants carried on P-selectin glycoprotein ligand 1 (PSGL-1), generally expressed on leukocytes (23). Furthermore, the E-selectin binding activity was significantly inhibited by anti-sLe^x antibody, anti-sLe^a antibody, or EDTA ($P < 0.000005$; Fig. S1), indicating that recombinant E-selectin did bind to the cells through the interaction with sLe$^{x/a}$.

We previously demonstrated that sLe$^{x/a}$ expressed on cancer cells promote tumor angiogenesis through interacting with E-selectin on endothelial cells (5). Because E-selectin is known to be induced by VEGF (24), we examined whether VEGF was secreted into the supernatant of the cells treated with EGF and/or bFGF. Results of ELISA indicated that the VEGF level was significantly increased by the treatment ($P < 0.0001$; Fig. 1*F*). These results suggest that EGF and/or bFGF can strongly promote angiogenesis synergistically by inducing sLe$^{x/a}$ and E-selectin expression on colon cancer cells and endothelial cells, respectively.

Altered Expression of *ST3GAL1/3/4*, *FUT3*, and *FUT2* Induced by EGF or bFGF. To address the molecular mechanism underlying the EMT-associated sLe$^{x/a}$ expression, we focused on the glycosyltrans-

ferase genes. Sialyltransferases and fucosyltransferases are essential enzymes for the synthesis of sialic acid and fucose residues of $sLe^{x/a}$, respectively. Screening of the genes involved in the $sLe^{x/a}$ synthesis by conventional RT-PCR using primers listed in Table S1 revealed that the levels of *ST3GAL1/3/4* and *FUT3/6* were increased, whereas that of *FUT2* was decreased by the EGF/bFGF treatment of HT29 and DLD-1 cells (Fig. 2*A*). Quantitation of the expression levels of these genes by real-time RT-PCR using the assays listed in Table S2 indicated that the EGF/bFGF treatment induced significant increases in the *ST3GAL1/3/4* and *FUT3* levels ($P < 0.005$; Fig. 2*B*) and a significant decrease in the *FUT2* level ($P < 0.00005$; Fig. 2*C*). In addition, these alterations were also induced by treatment with EGF or bFGF alone (Fig. 2 *B* and *C*). However, the *FUT6* level was not significantly changed by any of the treatment ($P > 0.05$; Fig. 2*B*). Therefore, we focused on *ST3GAL1/3/4*, *FUT3*, and *FUT2* for further experiments. ST3GAL1/3/4 catalyze the addition of *N*-acetylneuraminic acid (NeuAc) to the nonreducing terminal galactose (Gal) residue of glycans, and FUT3 catalyzes addition of fucose (Fuc) to the *N*-acetylglucosamine (GlcNAc) residue (Fig. 2*D*). Therefore, up-regulation of *ST3GAL1/3/4* and *FUT3* results in increased $sLe^{x/a}$ expression. In contrast, FUT2 catalyzes addition of Fuc to the nonreducing terminal Gal, competing with NeuAc addition by sialyltransferases (Fig. 2*D*). Down-regulation of *FUT2* thus contributes to increased $sLe^{x/a}$ expression. As expected, quantitative analysis by flow cytometry indicated that EGF/bFGF treatment induced significantly higher increase in the levels of sLe^x and sLe^a compared with those of Le^y and Le^b, respectively ($P < 0.01$; Fig. S2).

Involvement of c-Myc in the Induction of *ST3GAL1/3/4* and *FUT3* Expression by EGF/bFGF. To explore the mechanism of the EGF/bFGF-induced alteration in the glycogene transcription, we next searched for potential transcription factor binding sites in the 5′-regulatory regions of the glycogenes identified above and noticed potential c-Myc binding sites in the promoters of *ST3GAL1/3/4* and *FUT3* (Fig. S3 *A–D*). ChIP assays using primers listed in Table S3 indicated increased recruitment of c-Myc to their promoters in the EGF/bFGF-treated cells (Fig. 3*A*). To determine the role of c-Myc in the $sLe^{x/a}$ induction, we performed c-Myc knockdown experiments. Namely, we introduced a c-Myc shRNA-expressing vector into HT29 and DLD-1 cells (Fig. 3*B*) and treated the cells with EGF/bFGF. Knockdown of c-Myc significantly inhibited the maximal induction of *ST3GAL1/3/4* and *FUT3* expression ($P < 0.05$; Fig. 3*C*). Consequently, the maximal $sLe^{x/a}$ induction was also inhibited ($P < 0.0005$; Fig. 3*D*). These results suggested a pivotal role of c-Myc in the $sLe^{x/a}$ induction through the transcriptional regulation of *ST3GAL1/3/4* and *FUT3* under the EGF/bFGF treatment. To gain insights into the molecular mechanism by which the EGF/bFGF treatment induced the glycogenes through c-Myc, we performed Western blot analysis. Unexpectedly, the level of total c-Myc was reduced by the treatment in HT29 cells (Fig. 3*E*) likely caused by a decrease in the transcript level (Fig. 3*F*). However, the level of phospho–c-$Myc^{Ser62/Thr58}$ was strongly enhanced by the treatment both in HT29 and DLD-1 cells (Fig. 3*E*). It is known that a priming phosphorylation of c-Myc at Ser62 can be followed by phosphorylation at Thr58 by GSK3β (25). Because Western blotting revealed a decrease in the level of total GSK3β and an increase in that of phospho-$GSK3β^{Ser9}$, the inactivated form of GSK3β (Fig. S4), the increase in the phospho–c-$Myc^{Ser62/Thr58}$ level most likely reflects the hyperphosphorylation of the Ser62 site, which has been implicated in the enhanced recruitment of c-Myc to the promoter of its target

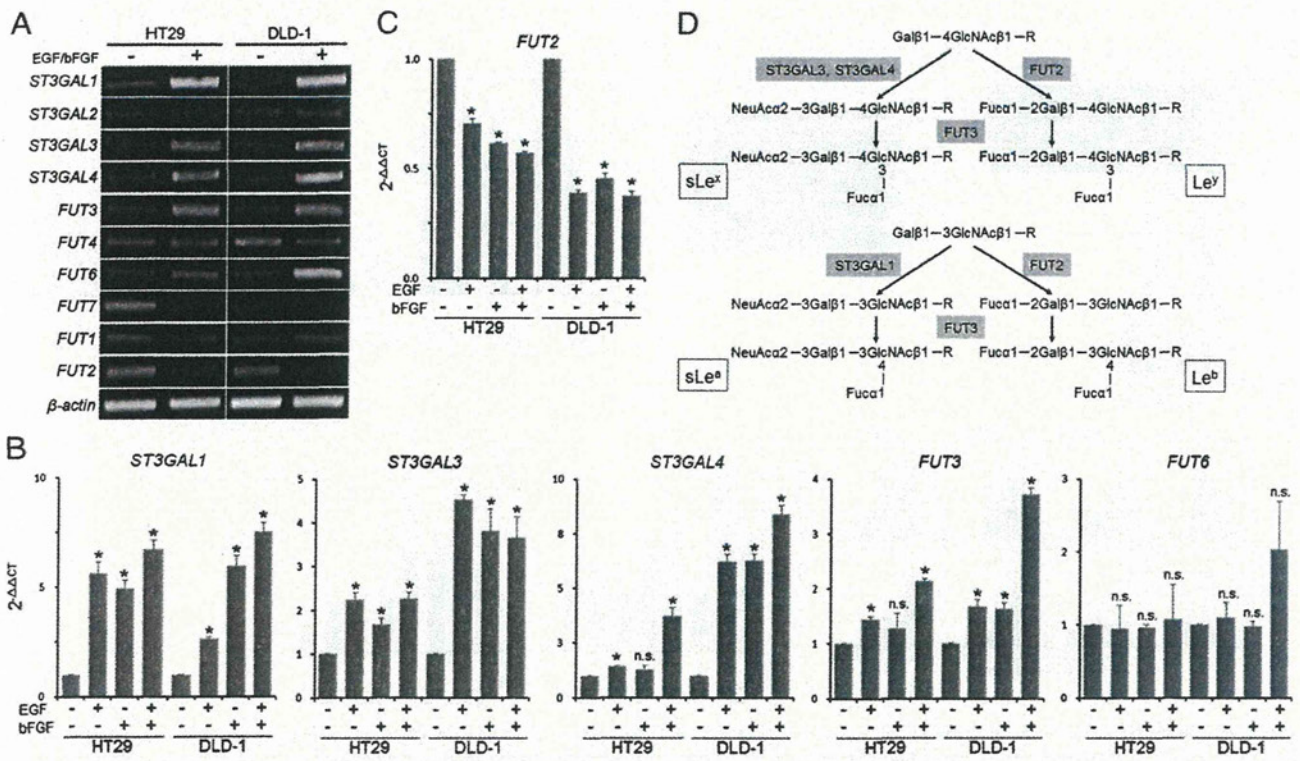

Fig. 2. Altered glycogene expression induced by EGF or bFGF. (*A*) Expression of the sialyltransferase and fucosyltransferase genes involved in the $sLe^{x/a}$ synthesis was screened by conventional RT-PCR. (*B* and *C*) Expression levels of *ST3GAL1/3/4*, *FUT3/6* (*B*), and *FUT2* (*C*) were determined by quantitative RT-PCR. The mean $2^{-\Delta\Delta CT}$ values ± SD from three independent experiments are shown. Statistic analysis was performed by *t* test. Asterisks, $P < 0.005$ (*B*) and $P < 0.00005$ (*C*) compared with the untreated cells; NS, not significant ($P > 0.05$). (*D*) Scheme of the sLe^x, Le^y, sLe^a, and Le^b synthetic pathways showing the roles of ST3GAL1/3/4, FUT3, and FUT2. Note that FUT2 competes with ST3GAL3/4 for sLe^x synthesis and with ST3GAL1 for sLe^a synthesis, respectively.

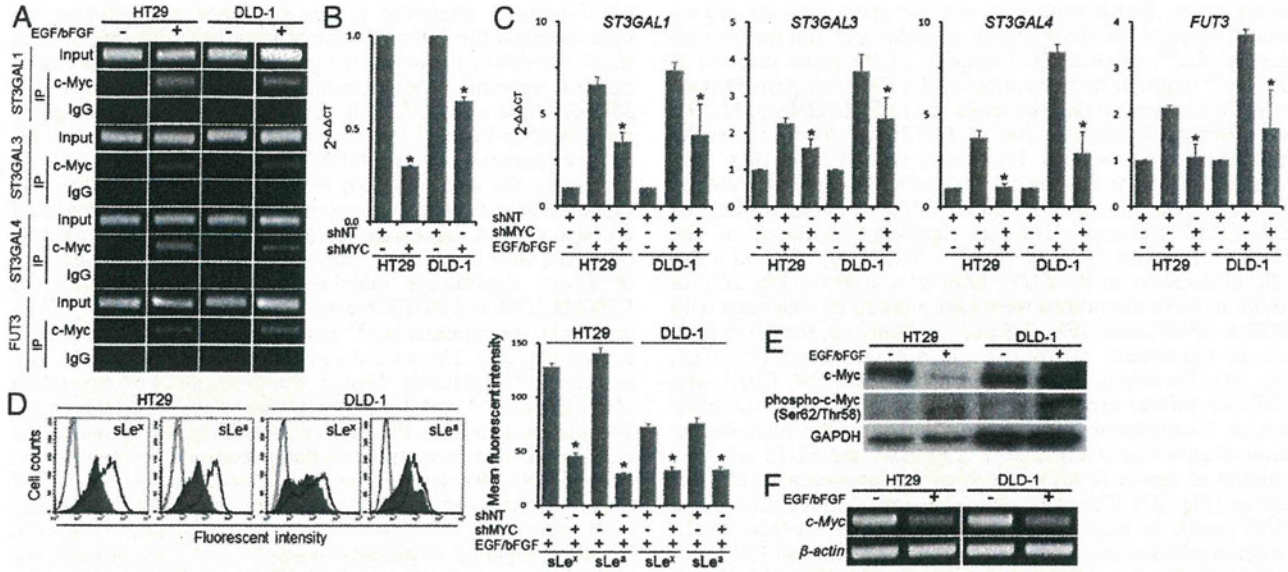

Fig. 3. Involvement of c-Myc in the transcriptional regulation of *ST3Gal1/3/4* and *FUT3*. (*A*) ChIP assays were performed to examine the binding of c-Myc to the 5′-regulatory regions of *ST3Gal1/3/4* and *FUT3*. (*B*) Effect of c-Myc shRNA (shMYC) on the transcript level of *c-Myc* was evaluated by quantitative RT-PCR. (*C*) Effects of shMYC on the expression levels of *ST3Gal1/3/4* and *FUT3* were examined by quantitative RT-PCR. (*D*) Expression levels of $sLe^{x/a}$ were examined by flow cytometry. Dotted lines, staining control; bold lines, nontarget shRNA (shNT)-introduced cells; filled histogram, shMYC-introduced cells. (*E*) Levels of c-Myc and phospho–c-$Myc^{Ser62/Thr58}$ were determined by Western blotting. (*F*) Expression of *c-Myc* was examined by conventional RT-PCR. (*B–D*) Statistic analysis was performed in three independent experiments by *t* test. Error bars, SD; asterisks, $P < 0.00001$ (*B*), $P < 0.05$ (*C*), and $P < 0.0005$ (*D*) compared with the shNT-transfected cells (*B*) or to the shNT-introduced cells treated with EGF/bFGF (*C* and *D*).

genes as well as in the enhanced transcriptional activity of c-Myc (26, 27).

Involvement of *CDX2* in the EGF/bFGF-Induced Transcriptional Suppression of *FUT2*. We next examined the mechanism of the

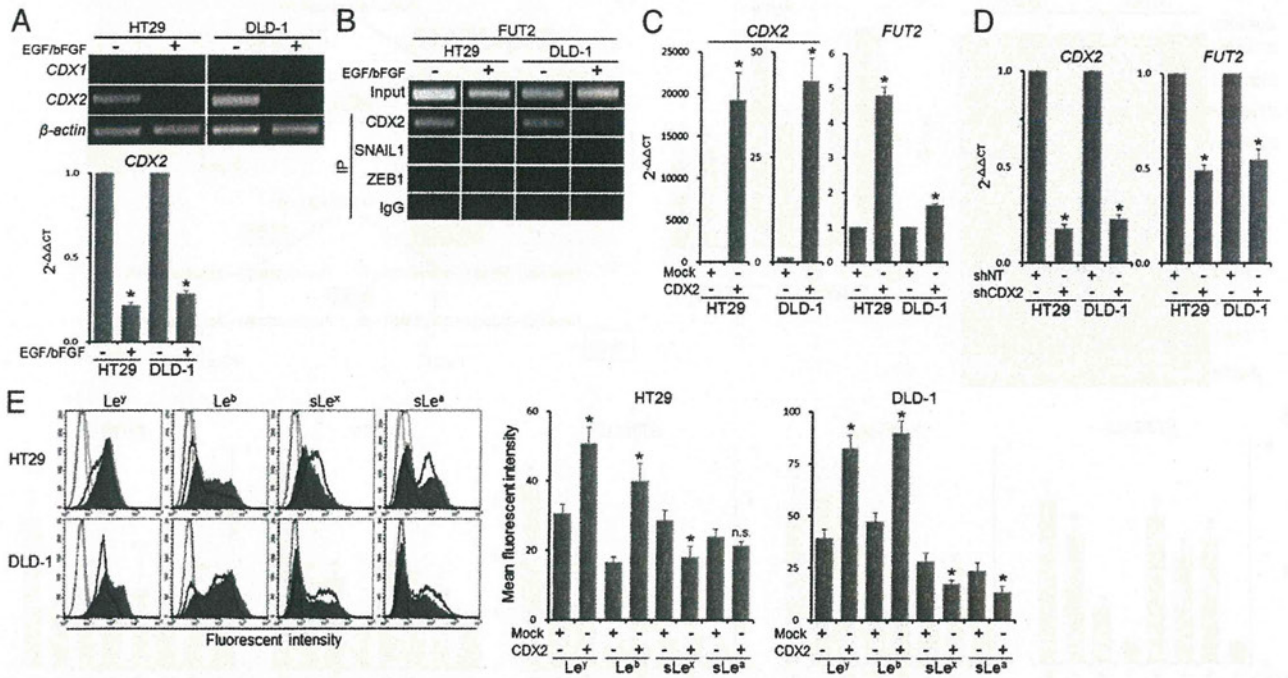

Fig. 4. Involvement of CDX2 in the transcriptional regulation of *FUT2*. (*A*) Expression of *CDX1* and *CDX2* was examined by conventional RT-PCR. The transcript level of *CDX2* was determined by quantitative RT-PCR. (*B*) ChIP assays were performed to examine the binding of CDX2, SNAIL1, and ZEB1 to the 5′-regulatory region of *FUT2*. (*C* and *D*) Effect of CDX2 forced expression (*C*) or CDX2 shRNA (shCDX2; *D*) on the expression levels of *CDX2* and *FUT2* were determined by quantitative RT-PCR. (*E*) Expression levels of $Le^{y/b}$ and $sLe^{x/a}$ were examined by flow cytometry. Dotted lines, staining control; bold lines, mock vector-introduced cells; filled histogram, CDX2 expression vector-introduced cells. (*A* and *C–E*) Statistic analysis was performed in three independent experiments by *t* test. Error bars, SD; asterisks, $P < 0.000001$ (*A*), $P < 0.0005$ (*C* and *D*), and $P < 0.05$ (*E*) compared with the untreated cells (*A*), to the mock vector-transfected cells (*C* and *E*) or to the nontarget shRNA (shNT)-transfected cells (*D*); NS, not significant ($P > 0.05$).

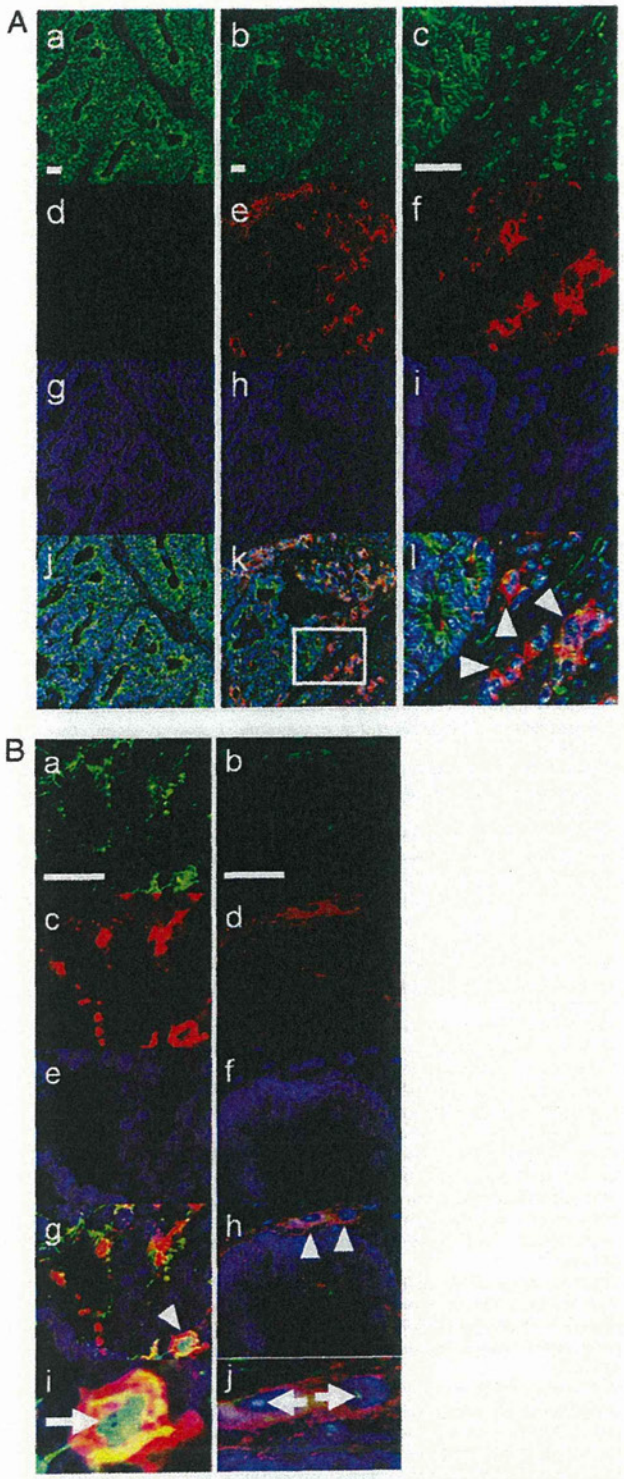

Fig. 5. E-selectin ligand glycan expression on colon cancer cells undergoing EMT in vivo. (*A*) Expression of E-cadherin (green) and sLe^a (red) was examined on human colon cancer sections by immunohistochemistry. (*Left*) Region with cancer cells exhibiting high cell-surface E-cadherin expression. (*Center*) Another region in the same section containing cancer cells without cell-surface E-cadherin expression, a part of which are surrounded by a square (*k*) and magnified in the *Right* column. Arrowheads indicate cells with decreased E-cadherin and increased sLe^a expression on the cell surface. (Blue) Hoechst 33342. (*B*) Expression of SNAIL1 (*a*, green), ZEB1 (*b*, green), and sLe^a (*c* and *d*, red) was examined on sections from the same patient. (*e* and *f*) Hoechst 33342. Cells with arrowheads (*g* and *h*) are magnified (*i* and *j*), with arrows showing nuclear SNAIL1 and ZEB1, respectively. (Scale bars, 50 μm.)

EGF/bFGF-induced transcriptional suppression of *FUT2*. We noticed potential binding sites for CDX1 and CDX2, transcription factors known to regulate several colon-specific genes (28–31), in the 5′-regulatory region of *FUT2* (Fig. S3*E*). Both HT29 and DLD-1 cells showed good levels of *CDX2* expression, which were significantly reduced by EGF/bFGF treatment ($P < 0.000001$; Fig. 4*A*). ChIP assays revealed that binding of CDX2 to the *FUT2* promoter was abolished by the treatment (Fig. 4*B*). On the other hand, SNAIL1 and ZEB1, EMT-related transcriptional repressors, were not recruited to the promoter (Fig. 4*B*). To determine the role of CDX2 in the transcriptional regulation of *FUT2*, we introduced a CDX2 expression vector into HT29 and DLD-1 cells. The cells exhibited significantly elevated *FUT2* expression compared with the mock vector-transfected cells ($P < 0.0005$; Fig. 4*C*). In contrast, HT29 and DLD-1 cells introduced with CDX2 shRNA showed significantly reduced level of *FUT2* ($P < 0.0005$; Fig. 4*D*). Furthermore, forced expression of *CDX2* elevated Le$^{y/b}$ expression and suppressed sLe$^{x/a}$ expression in HT29 and DLD-1 cells (Fig. 4*E*). These results suggest that the EGF/bFGF-induced down-regulation of *CDX2* contributes to the sLe$^{x/a}$ induction via suppression of *FUT2* transcription.

E-Selectin Ligand Glycan Expression on Colon Cancer Cells Undergoing EMT in Vivo. Finally, we examined association between E-selectin ligand glycan expression and EMT in clinial samples by immunohistochemical analysis. We focused on sLe^a in this experiment, because this glycan is preferentially expressed on cancer cells, whereas sLe^x is broadly expressed on various normal cells including leukocytes and might complicate the results. We performed double staining with antibodies against sLe^a and E-cadherin on sections from five colorectal cancer patients. In one section from a 70-y-old male patient with colon cancer, we identified a small area of cancer cells that lacked cell-surface E-cadherin expression at the invasion front (Fig. 5*A*). Most interestingly, these cancer cells exhibited high sLe^a expression, whereas cancer cells with cell-surface E-cadherin exhibited no sLe^a expression (Fig. 5*A*). Furthermore, double staining with antibodies against SNAIL1 and sLe^a identified a subset of cancer cells that coexpressed nuclear SNAIL1 and a high level of sLe^a (Fig. 5*B*). Similar results were obtained by double staining with antibodies against ZEB1 and sLe^a (Fig. 5*B*). These results supported the coincidence of E-selectin ligand expression and EMT observed in vitro.

Discussion

The major findings of this study are as follows: (*i*) sLe$^{x/a}$ expression is strongly induced during EMT of colon cancer cells triggered by EGF or bFGF, and (*ii*) c-Myc and CDX2 play key roles in the sLe$^{x/a}$ induction by EGF or bFGF.

Our present results demonstrate that c-Myc contributes to sLe$^{x/a}$ expression by transcriptional induction of *ST3GAL1/3/4* and *FUT3* in the EGF/bFGF-treated cells. Although the detailed mechanism of this glycogene induction by c-Myc remains unclear, we speculate the possible involvement of Ser62 phosphorylation of c-Myc as described above (Fig. 3*E*). Ser62 of c-Myc is known to be phosphorylated by ERK or cyclin-dependent kinase (CDK) 2 (25–27). The kinase that contributed to this phosphorylation in the EGF/bFGF-treated cells remains to be identified.

In this study, we demonstrated that the transcription of *CDX2* was down-regulated by the EGF/bFGF treatment, which resulted in a decrease in the transcript level of *FUT2*. Although the mechanism underlying the down-regulation of *CDX2* by the treatment remains unknown, SNAIL1 may be involved because transcription of *CDX2* is known to be repressed by SNAIL1 (32), and *SNAIL1* expression was increased by EGF/bFGF (Fig. 1*B*). Although several lines of evidence indicate that CDX2 is a tumor suppressor (33), the association between CDX2 and metastasis

has been unclear. Clinically, Baba et al. reported that the loss of CDX2 expression in colon cancer tissues was significantly correlated with stage IV disease (34). Our present findings may explain at least a part of the mechanisms by which the loss of CDX2 contributes to metastasis.

We previously reported that hypoxia induced $sLe^{x/a}$ expression in colon cancer cells (9). In that report, we documented that the transcription of *ST3GAL1*, *FUT7*, and *UGT1* (UDP-galactose transporter 1), which are all involved in the E-selectin ligand glycan synthesis, was elevated under a hypoxic condition. Hypoxia-inducible factor-1α (HIF-1α) was involved in the induction of these glycogenes. The present study provides additional information on the transcriptional regulation of the $sLe^{x/a}$ synthesis-related glycogenes.

Recently, Guan et al. reported a significant association between glycans and EMT, demonstrating that the expression levels of GM2 and Gg4 glycosphingolipids were significantly decreased during TGF-β–induced EMT and that the glucosylceramide synthase inhibitor EtDO-P4 induced EMT (35). From their subsequent observations demonstrating that exogenous addition of Gg4 abrogated the EMT process and that Gg4 was closely associated with E-cadherin and β-catenin, they proposed that Gg4 may be important in maintaining epithelial cell membrane organization (36). Together with these reports, our present study demonstrates a drastic alteration in the glycan expression during the EMT process. It remains an interesting issue whether the alteration in $sLe^{x/a}$ expression further promotes the EMT process as the alteration in the Gg4 expression did.

We demonstrated that sLe^{a} was preferentially expressed on the cancer cells with low expression of membranous E-cadherin, nuclear SNAIL1, and nuclear ZEB1 in a clinical sample of colon cancer. These results are consistent with the coincidence of $sLe^{x/a}$ expression and EMT observed in vitro and suggest that these glycans may serve as a good marker of EMT in cancer patients. Our results indicate that RTK signaling activation confers both EMT and $sLe^{x/a}$ expression on cancer cells. As RTK signaling pathways provide effective therapeutic targets, these glycans may serve as surrogate markers for evaluating therapeutic effects of such modalities.

Materials and Methods

Additional information can be found in *SI Materials and Methods*.

Human colon cancer cell lines, HT29 and DLD-1, were maintained in DMEM and RPMI1640 medium (Invitrogen), respectively, supplemented with 10% (vol/vol) FBS. For treatment with EGF and/or bFGF, recombinant human EGF (Sigma; 20 ng/mL) and/or recombinant human bFGF (Sigma; 10 ng/mL) were added to the serum-free medium with recombinant human insulin (Sigma; 25 μg/mL), human holo-transferrin (Sigma; 100 μg/mL), putrescine dihydrochloride (Sigma; 10 μg/mL), and sodium selenite (Sigma; 5 ng/mL).

ACKNOWLEDGMENTS. This work was supported in part by Grants-in-Aid for Young Scientists (B) 20790583 and 22790774 from the Japan Society for the Promotion of Science, Grants-in-Aid 24590364 and (on priority areas) 23112520 from the Ministry of Education, Culture, Sports, Science and Technology, Grants-in-Aid for the Third-Term Comprehensive Ten-Year Strategy for Cancer Control from the Ministry of Health and Welfare, and a grant from Uehara Memorial Foundation, Japan.

1. Jemal A, et al. (2011) Global cancer statistics. *CA Cancer J Clin* 61:69–90.
2. Kannagi R (1997) Carbohydrate-mediated cell adhesion involved in hematogenous metastasis of cancer. *Glycoconj J* 14:577–584.
3. Kannagi R, Izawa M, Koike T, Miyazaki K, Kimura N (2004) Carbohydrate-mediated cell adhesion in cancer metastasis and angiogenesis. *Cancer Sci* 95:377–384.
4. Takada A, et al. (1993) Contribution of carbohydrate antigens sialyl Lewis A and sialyl Lewis X to adhesion of human cancer cells to vascular endothelium. *Cancer Res* 53: 354–361.
5. Tei K, et al. (2002) Roles of cell adhesion molecules in tumor angiogenesis induced by cotransplantation of cancer and endothelial cells to nude rats. *Cancer Res* 62:6289–6296.
6. Carmeliet P, Jain RK (2000) Angiogenesis in cancer and other diseases. *Nature* 407: 249–257.
7. Tien YW, et al. (2001) Tumor angiogenesis and its possible role in intravasation of colorectal epithelial cells. *Clin Cancer Res* 7:1627–1632.
8. Zetter BR (1998) Angiogenesis and tumor metastasis. *Annu Rev Med* 49:407–424.
9. Koike T, et al. (2004) Hypoxia induces adhesion molecules on cancer cells: A missing link between Warburg effect and induction of selectin-ligand carbohydrates. *Proc Natl Acad Sci USA* 101:8132–8137.
10. Miyazaki K, et al. (2004) Loss of disialyl Lewis(a), the ligand for lymphocyte inhibitory receptor sialic acid-binding immunoglobulin-like lectin-7 (Siglec-7) associated with increased sialyl Lewis(a) expression on human colon cancers. *Cancer Res* 64: 4498–4505.
11. Yusa A, Miyazaki K, Kimura N, Izawa M, Kannagi R (2010) Epigenetic silencing of the sulfate transporter gene DTDST induces sialyl Lewisx expression and accelerates proliferation of colon cancer cells. *Cancer Res* 70:4064–4073.
12. Kalluri R, Weinberg RA (2009) The basics of epithelial-mesenchymal transition. *J Clin Invest* 119:1420–1428.
13. Thiery JP, Acloque H, Huang RY, Nieto MA (2009) Epithelial-mesenchymal transitions in development and disease. *Cell* 139:871–890.
14. Mani SA, et al. (2008) The epithelial-mesenchymal transition generates cells with properties of stem cells. *Cell* 133:704–715.
15. Radisky DC, LaBarge MA (2008) Epithelial-mesenchymal transition and the stem cell phenotype. *Cell Stem Cell* 2:511–512.
16. Ikushima H, Miyazono K (2010) TGFbeta signalling: A complex web in cancer progression. *Nat Rev Cancer* 10:415–424.
17. Xu Y, Pasche B (2007) TGF-beta signaling alterations and susceptibility to colorectal cancer. *Hum Mol Genet* 16(Spec No 1):R14–R20.
18. Normanno N, et al. (2009) Implications for KRAS status and EGFR-targeted therapies in metastatic CRC. *Nat Rev Clin Oncol* 6:519–527.
19. Radinsky R, et al. (1995) Level and function of epidermal growth factor receptor predict the metastatic potential of human colon carcinoma cells. *Clin Cancer Res* 1: 19–31.
20. Goldstein NS, Armin M (2001) Epidermal growth factor receptor immunohistochemical reactivity in patients with American Joint Committee on Cancer Stage IV colon adenocarcinoma: Implications for a standardized scoring system. *Cancer* 92: 1331–1346.
21. George ML, Tutton MG, Abulafi AM, Eccles SA, Swift RI (2002) Plasma basic fibroblast growth factor levels in colorectal cancer: A clinically useful assay? *Clin Exp Metastasis* 19:735–738.
22. Sato T, et al. (2009) Overexpression of the fibroblast growth factor receptor-1 gene correlates with liver metastasis in colorectal cancer. *Oncol Rep* 21:211–216.
23. McEver RP, Cummings RD (1997) Perspectives series: Cell adhesion in vascular biology. Role of PSGL-1 binding to selectins in leukocyte recruitment. *J Clin Invest* 100: 485–491.
24. Kim I, et al. (2001) Vascular endothelial growth factor expression of intercellular adhesion molecule 1 (ICAM-1), vascular cell adhesion molecule 1 (VCAM-1), and E-selectin through nuclear factor-kappa B activation in endothelial cells. *J Biol Chem* 276:7614–7620.
25. Sears R, et al. (2000) Multiple Ras-dependent phosphorylation pathways regulate Myc protein stability. *Genes Dev* 14:2501–2514.
26. Benassi B, et al. (2006) c-Myc phosphorylation is required for cellular response to oxidative stress. *Mol Cell* 21:509–519.
27. Hydbring P, et al. (2010) Phosphorylation by Cdk2 is required for Myc to repress Ras-induced senescence in cotransformation. *Proc Natl Acad Sci USA* 107:58–63.
28. Dang DT, Mahatan CS, Dang LH, Agboola IA, Yang VW (2001) Expression of the gut-enriched Krüppel-like factor (Krüppel-like factor 4) gene in the human colon cancer cell line RKO is dependent on CDX2. *Oncogene* 20:4884–4890.
29. Yamamoto H, Bai YQ, Yuasa Y (2003) Homeodomain protein CDX2 regulates goblet-specific MUC2 gene expression. *Biochem Biophys Res Commun* 300: 813–818.
30. Chan CW, et al. (2009) Gastrointestinal differentiation marker Cytokeratin 20 is regulated by homeobox gene CDX1. *Proc Natl Acad Sci USA* 106:1936–1941.
31. Kakizaki F, et al. (2010) CDX transcription factors positively regulate expression of solute carrier family 5, member 8 in the colonic epithelium. *Gastroenterology* 138: 627–635.
32. Gross I, et al. (2008) The intestine-specific homeobox gene Cdx2 decreases mobility and antagonizes dissemination of colon cancer cells. *Oncogene* 27:107–115.
33. Guo RJ, Suh ER, Lynch JP (2004) The role of Cdx proteins in intestinal development and cancer. *Cancer Biol Ther* 3:593–601.
34. Baba Y, et al. (2009) Relationship of CDX2 loss with molecular features and prognosis in colorectal cancer. *Clin Cancer Res* 15:4665–4673.
35. Guan F, Handa K, Hakomori SI (2009) Specific glycosphingolipids mediate epithelial-to-mesenchymal transition of human and mouse epithelial cell lines. *Proc Natl Acad Sci USA* 106:7461–7466.
36. Guan F, Schaffer L, Handa K, Hakomori SI (2010) Functional role of gangliotetraosylceramide in epithelial-to-mesenchymal transition process induced by hypoxia and by TGF-β. *FASEB J* 24(12):4889–4903.

Supporting Information

Sakuma et al. 10.1073/pnas.1111135109

SI Materials and Methods

Antibodies and Reagents. Monoclonal antibodies against sLe^x (clone SNH-3, murine IgM), sLe^a (clone 2D3, murine IgM), and Le^y (clone AH-6, murine IgM) were prepared as described previously (1–3). Anti-Le^b antibody (clone 2-25LE, murine IgG1) was obtained from Seikagaku Biobusiness. Recombinant human E/P-selectins Fc chimera and FITC-conjugated antihuman IgG Fc antibody were obtained from R&D Systems and Sigma, respectively. Antibodies against c-Myc (clone 9E11) and SNAIL1, those against CDX2 and ZEB1, and those against phospho–c-$Myc^{Ser62/Thr58}$ and phospho-$GSK3\beta^{Ser9}$ (clone D85E12) were obtained from Abcam, Santa Cruz, and Cell Signaling Technology, respectively.

Flow Cytometry. For flow cytometric analyses, cells were harvested and stained with respective primary antibodies using culture supernatants at a dilution of 1:5 or purified antibodies at 1 μg/mL. The cells were then stained with a 1:300 dilution of FITC-conjugated secondary antibody. For selectin-binding assays, cells were incubated with recombinant selectins at 20 μg/mL followed by incubation with FITC-conjugated secondary antibody at 2 μg/mL, with all of the reactions performed in calcium containing Dulbecco's PBS except experiments in the presence of EDTA at a final concentration of 1 mM. For blocking experiments, cells were pretreated with SNH-3 and/or 2D3 antibodies at a final concentration of 100 μg/mL before incubation with recombinant selectins. Propidium iodide was used at 1 μg/mL to identify living cells. Cells were analyzed with a FACSCalibur (BD Biosciences).

Conventional and Quantitative RT-PCR Analysis. Total cellular RNA was isolated with ISOGEN reagent (Nippon Gene). First strand cDNA was prepared from the total RNA (5 μg) with SuperScript II Reverse Transcriptase (Invitrogen). Conventional RT-PCR analysis was performed with KOD-Plus- (Toyobo) and primers listed in Table S1 using a GeneAmp PCR system 9700 (Applied Biosystems). For quantitative RT-PCR, cDNA samples were mixed with FAM-labeled TaqMan gene expression assays (Table S2), VIC-labeled TaqMan MGB probe for β-actin, and TaqMan gene expression master mix (Applied Biosystems), followed by amplification using 7500 Fast Real-Time PCR system (Applied Biosystems) according to the manufacturer's protocol. Results were calculated by the comparative CT method, with relative transcript levels determined as $2^{-\Delta\Delta CT}$.

ChIP Assay. Chromatin samples were isolated from cells with a ChIP-IT Express kit (Active Motif) according to the manufacturer's protocol. Samples (60 μL) were incubated with antibodies (1 μg) for 8 h at 4 °C. The primers for detection of the promoter sequences were designed in the 5′-regulatory regions of *ST3GAL1/3/4*, *FUT3*, and *FUT2*, all of which were previously reported (4–9). The primers used are listed in Table S3.

RNA Knockdown and Forced Expression. The pLKO.1-based lentiviral shRNA, the nontarget shRNA, packaging and envelope plasmids were obtained from Sigma. The plasmids were co-transfected into HEK293T cells to produce viral particles using FuGENE 6 (Promega). HT29 and DLD-1 cells were infected with the viral supernatants in the presence of 8 μg/mL of polybrene (Sigma). After selection with 5 μg/mL of puromycin (Sigma), total RNA was extracted and analyzed by quantitative RT-PCR. For c-Myc knockdown, TRCN0000010389 having the sequence CCGGAACTATGACCTCGACTACGACTCGAGTCGTAGTCGAGGTCATAGTTCTTTTTG gave the best results among the five tested shRNA vectors. For CDX2 knockdown, TRCN0000013687 having the sequence CCGGAGCCCTTGAGTCCGGTGTCTTCTCGAGAAGACACCGGACTCAAGGGCTTTTTT gave the best results among the five tested shRNA vectors. For CDX2 forced expression, a cDNA expression vector was purchased from OriGene and introduced into HT29 and DLD-1 cells using FuGENE 6 reagent. After a 3-d culture, total RNA was extracted and analyzed by quantitative RT-PCR.

Cell Migration Assay. Cell migration activity was determined using Biocoat Matrigel invasion chambers (BD Biosciences) according to the manufacturer's instructions. Briefly, cells (2×10^5) were seeded in serum-free culture medium onto the Matrigel-coated filters. Culture medium supplemented with 10% (vol/vol) FBS was added to the lower part of the chambers. After a 24-h incubation period at 37 °C, the filters were stained with Diff-Quik dye (Sysmex International Reagents) and migrated cells were counted in five randomly chosen fields under a light microscope.

ELISA. Culture supernatant VEGF levels were measured by ELISA using a Milliplex MAP Human Cytokine/Chemokine kit (Millipore). Samples were collected on the third day from the medium replacement and subjected to ELISA at a dilution of 1:4. All of the assays were performed in triplicate.

Western Blotting. Cell lysates were prepared with RIPA buffer (Thermo Scientific) containing blends of protease and phosphatase inhibitors (Roche Applied Science). Samples were subjected to SDS/PAGE, followed by transfer onto PVDF membrane (Bio-Rad). After blocking, the blots were incubated with primary antibodies and HRP-conjugated secondary antibody (SouthernBiotech) at appropriate dilutions. The signal was detected with an ECL kit (GE Healthcare).

Immunohistochemistry. Colon cancer tissues were obtained from patients in Kyoto University Hospital under informed consent, and investigations were conducted according to the Declaration of Helsinki principles. Frozen sections of 10-μm thickness were fixed with ice-cold acetone. After blocking with PBS(−) including 5% (vol/vol) normal goat serum and 0.3% Triton X-100 for 60 min, the sections were incubated with primary and secondary antibodies, and Hoechst 33342 (Dojindo) according to the manufacturer's instructions. Stained sections were observed with a LSM510 confocal microscope (Carl Zeiss).

1. Abe K, McKibbin JM, Hakomori S (1983) The monoclonal antibody directed to difucosylated type 2 chain (Fuc alpha 1 leads to 2Gal beta 1 leads to 4[Fuc alpha 1 leads to 3]GlcNAc; Y Determinant). *J Biol Chem* 258:11793–11797.
2. Phillips ML, et al. (1990) ELAM-1 mediates cell adhesion by recognition of a carbohydrate ligand, sialyl-Lex. *Science* 250:1130–1132.
3. Takada A, et al. (1991) Adhesion of human cancer cells to vascular endothelium mediated by a carbohydrate antigen, sialyl Lewis A. *Biochem Biophys Res Commun* 179:713–719.
4. Taniguchi A, Yoshikawa I, Matsumoto K (2001) Genomic structure and transcriptional regulation of human Galbeta1,3GalNAc alpha2,3-sialyltransferase (hST3Gal I) gene. *Glycobiology* 11:241–247.

5. Taniguchi A, Saito K, Kubota T, Matsumoto K (2003) Characterization of the promoter region of the human Galbeta1,3(4)GlcNAc alpha2,3-sialyltransferase III (hST3Gal III) gene. *Biochim Biophys Acta* 1626:92–96.
6. Taniguchi A, Matsumoto K (1999) Epithelial-cell-specific transcriptional regulation of human Galbeta1,3GalNAc/Galbeta1,4GlcNAc alpha2,3-sialyltransferase (hST3Gal IV) gene. *Biochem Biophys Res Commun* 257:516–522.
7. Cameron HS, Szczepaniak D, Weston BW (1995) Expression of human chromosome 19p alpha(1,3)-fucosyltransferase genes in normal tissues. Alternative splicing, polyadenylation, and isoforms. *J Biol Chem* 270:20112–20122.
8. Dabrowska A, Baczyńska D, Widerak K, Laskowska A, Ugorski M (2005) Promoter analysis of the human alpha1,3/4-fucosyltransferase gene (FUT III). *Biochim Biophys Acta* 1731:66–73.
9. Koda Y, Soejima M, Wang B, Kimura H (1997) Structure and expression of the gene encoding secretor-type galactoside 2-alpha-L-fucosyltransferase (FUT2). *Eur J Biochem* 246:750–755.

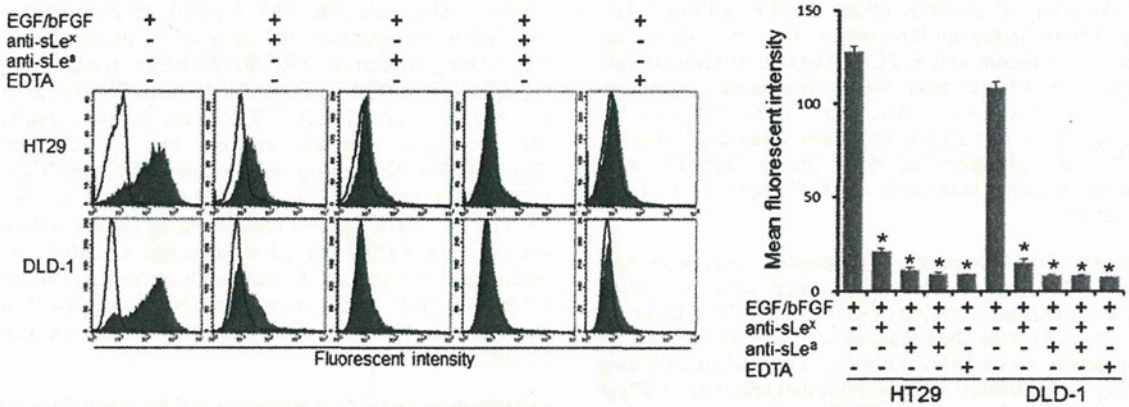

Fig. S1. Contribution of $sLe^{x/a}$ to E-selectin binding activity. E-selectin binding activity was examined by flow cytometry using recombinant E-selectin. The EGF/bFGF-treated cells were pretreated with or without anti-sLe^x and/or anti-sLe^a antibodies at a final concentration of 100 μg/mL or pretreated with or without 1 mM EDTA before incubation with recombinant E-selectin. Recombinant P-selectin was used as a negative control. Statistic analysis was performed in three independent experiments by *t* test. Bold lines, staining control; error bars, SD; asterisks, $P < 0.000005$ compared with the cells without pretreatment.

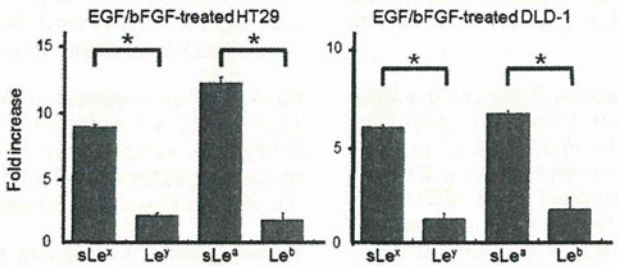

Fig. S2. Contribution of *FUT2* down-regulation to the preferential increase of $sLe^{x/a}$ compared with $Le^{y/b}$. Expression levels of sLe^x, Le^y, sLe^a, and Le^b were determined by flow cytometry. Results from three independent experiments are shown by fold increases of the mean fluorescent intensity in the EGF/bFGF-treated cells compared with that in the untreated cells. Statistic analysis was performed in three independent experiments by *t* test. Error bars, SD; asterisks, $P < 0.01$.

A ST3GAL1

TTCCTTAGCCCCGCCAGCTTGAGGGCCG
CGTCCAGAGAGCGGGGAGCTCCTCTCGG
GGCGCCGATCAGGTCCCCGCGCCGCAGC
CGCCGCCTCCGGCGTCTCCCAGGCTCGG
CCTCTGCCGAGCCCGCTGCGGTCCACGT
GGCTTGGCAGAGCTAAATTCGGCTTGCAG
GAAGCCCGGAGCCAAGGGAAAGCCGAG
CCAAGTTGGGGTG

B ST3GAL3

AGTGGCCGTGACTACCCTAGCACTTTGC
GTTCCCCGCGCGGGCGACGAAACACGCT
CTCGAGGGGAGAGAGCCGTGCGTCCTCT
GGGCCGTGAAGCCAGGGGAAGAGGGTTC
CTCTAGACAGCTCGATGTGCCCGGGAGA
GACACCCACGCTGAACCTGCAAGCTGGG
GTGCTCCACCAGCGCGAACCTCTCGCCC
CGCACTCGCCGCAGCACTGCTCTCGTGG
TAGGCGGGGTGGGCGGGACGGCAAATCC
GCGGCTCCTGCGTCTA

C ST3GAL4

GGCTCACCTGGATCCTTAATGCCGCCCT
TGGAGGAGTTAGGAGGATCCTGGATGAG
AAAACTCACCCTCAGGATGATTGCCCCCA
GGGAGCAGCTTCCTGCTTTCTGGTGGAAG
GGAGGGGCAGACAGTGGGTGTGTCCTGC
TCCAGTGTCTAGGCAGGAGAGTTTGTGAA
GCTGACCGGACACCTGTG

D FUT3

GGTCTCACAGGCGAGATTAGGACACCCC
GGAAACTGGCTTCCAGACAATATCCCTGC
TGCAGGGGAGAACACCCTAGGTCACCTG
GTGACAGGTGTGTGCTGCAATGTACACGT
ACTTGTTCC

E FUT2

CTTTCTGTTGGGGCATCACAACAGTTCCC
CAAGGAAGACCCTCGGGGACCCGGATGG
GGGATGCGACCTTGTCCTGCCTCTCTCCC
CCACCCTTATGGCCAGGCTTGGGGTGCCT
GGTGCAGGTGGAGGAGCTAAGGGTAGAT
AACAAGATGGACTTTGTGGCCG

Fig. S3. 5′-regulatory regions of *ST3GAL1/3/4*, *FUT3*, and *FUT2*. (*A–E*) DNA sequences of the 5′-regulatory regions of *ST3GAL1/3/4*, *FUT3*, and *FUT2* are shown. Bold letters, primer-targeted sequences for ChIP assay; single underlines, potential c-Myc binding sites; double underlines, potential binding sites for CDX1 and CDX2.

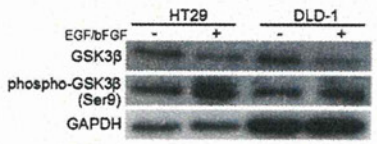

Fig. S4. EGF/bFGF-induced alteration in the levels of GSK3β and phospho-GSK3β^{Ser9}. The levels of GSK3β and phospho-GSK3β^{Ser9} in the untreated and EGF/bFGF-treated cells were determined by Western blotting.

Table S1. Primers used for conventional RT-PCR

Gene	Primer sequence	Length	Annealing, °C	Cycles
β-actin	F: CGTGCGTGACATTAAGGAGAAGC R: CAATGCCAGGGTACATGGTGGT	305	57	22
ST3GAL1	F: TGGTCCTGGAGCTCTCCGAGAA R: GACTGTCTATCTCAGGCCCATAAGAAGA	363	58	30
ST3GAL2	F: GATGATGCTGCAGCCCCAGTTC R: ACATCCTGCTCAAAGCCCACGGTT	237	58	30
ST3GAL3	F: CGGATGGCTTCTGGAAATCTGT R: TTGTGCGTCCAGGACTCTTTGA	300	55	30
ST3GAL4	F: TCCAGGGTGAGGCAGAGAGCAA R: TTGGGGATGGAGGAGCTGGTGA	190	58	27
FUT1	F: CACGAAAAGCGGACTGTGGATCTG R: GACACAGGATCGACAGGCCTAG	172	58	31
FUT2	F: CCTTCAGCAGGACCAGGTGAGA R: GGTCCCAGTGCCTTTGATGTTGAG	198	58	31
FUT3	F: TGTTTCTTCTCCTACCTGCGTGTGTC R: GTGTCTGCCTGTGGGTACACCT	230	58	30
FUT4	F: CAACATGTGACCGTGGACGTGTTC R: GGTGATATAATCCAGGTGCTGCGAGTT	135	58	27
FUT6	F: CATCTCAAGGTGGACGTGTACGGA R: GGTGGCAGGAACCTCTCGTAGT	215	58	30
FUT7	F: CCTGGGAGACTGTGGATGAATAATGCT R: GTGCCAGACAAGGATGGTGATCGT	174	58	32
E-cadherin	F: CAGAGCCTCTGGATAGAGAACGCA R: GGCATTGTAGGTGTTCACATCATCGTC	245	58	30
SNAIL1	F: TATGCTGCCTTCCCAGGCTTG R: ATGTGCATCTTGAGGGCACCC	143	57	30
ZEB1	F: CCAGTGGTCATGATGAAAATGGAACACC R: CAGACTGCGTCACATGTCTTTGATCTC	243	58	33
Vimentin	F: GGCTCAGATTCAGGAACAGC R: CTGAATCTCATCCTGCAGGC	373	55	30
MUC2	F: CCGTCCTCCTACCACATCAT R: CTCTCCAGGCCGTTGAAGT	149	55	30
ALPI	F: GCAACCCTGCAACCCACCCAAGGA R: CCAGCATCCAGATGTCCCGGGAG	278	62	30
c-Myc	F: TCCGTCCTCGGATTCTCTGCTCT R: GCCTCCAGCAGAAGGTGATCCA	208	58	30
CDX1	F: AGGACAAGTACCGCGTGGTCTA R: CCTCTGAACGTATGGAGGAGGA	670	57	35
CDX2	F: CAGTCGCTACATCACCATCCG R: GCAGAGTCCACGCTCCTCAT	384	57	28

F, forward primer; R, reverse primer.

Table S2. TaqMan gene expression assays used for quantitative RT-PCR

Gene	Assay ID
ST3GAL1	Hs00161688_m1
ST3GAL3	Hs00544033_m1
ST3GAL4	Hs00920871_m1
FUT2	Hs00704693_s1
FUT3	Hs01868572_s1
FUT6	Hs03026676_s1
c-Myc	Hs00905030_m1
CDX2	Hs01078080_m1

Table S3. Primers used for ChIP assay

Gene	Primer sequence	Product length	Annealing, °C
ST3GAL1	F: TTCCTTAGCCCCGCCAGCTTGA R: CACCCCAACTTGGCTCGGCTTT	209	58
ST3GAL3	F: AGTGGCCGTGACTACCCTAGCAC R: TAGACGCAGGAGCCGCGGATT	268	62
ST3GAL4	F: GGCTCACCTGGATCCTTAATGCC R: CACAGGTGTCCGGTCAGCTTCA	189	58
FUT2	F: CTTTCTGTTGGGGCATCACAACAGTTC R: CGGCCACAAAGTCCATCTTGTTATCTAC	165	58
FUT3	F: GGTCTCACAGGCGAGATTAGGACA R: GGAACAAGTACGTGTACATTGCAGCACA	123	58

F, forward primer; R, reverse primer.

DNA Repair 11 (2012) 259–266

Contents lists available at SciVerse ScienceDirect

DNA Repair

journal homepage: www.elsevier.com/locate/dnarepair

Activation of AMP-activated protein kinase by MAPO1 and FLCN induces apoptosis triggered by alkylated base mismatch in DNA

Teik How Lim[a], Ryosuke Fujikane[b], Shiori Sano[b,c], Ryuji Sakagami[c], Yoshimichi Nakatsu[a], Teruhisa Tsuzuki[a], Mutsuo Sekiguchi[d], Masumi Hidaka[b,*]

[a] Department of Medical Biophysics and Radiation Biology, Faculty of Medical Sciences, Kyushu University, Fukuoka 812-8582, Japan
[b] Department of Physiological Science and Molecular Biology, Fukuoka Dental College, Fukuoka 814-0193, Japan
[c] Department of Odontology, Fukuoka Dental College, Fukuoka 814-0193, Japan
[d] Frontier Research Center, Fukuoka Dental College, Fukuoka 814-0193, Japan

ARTICLE INFO

Article history:
Received 31 August 2011
Received in revised form 9 November 2011
Accepted 28 November 2011
Available online 29 December 2011

Keywords:
AMPK
Apoptosis
Folliculin/BHD
MAPO1/FNIP2/FNIPL
O^6-methylguanine

ABSTRACT

O^6-Methylguanine produced in DNA by the action of simple alkylating agents, such as *N*-methyl-*N*-nitrosourea (MNU), causes base-mispairing during DNA replication, thus leading to mutations and cancer. To prevent such outcomes, the cells carrying O^6-methylguanine undergo apoptosis in a mismatch repair protein-dependent manner. We previously identified MAPO1 as one of the components required for the induction of apoptosis triggered by O^6-methylguanine. MAPO1, also known as FNIP2 and FNIPL, forms a complex with AMP-activated protein kinase (AMPK) and folliculin (FLCN), which is encoded by the *BHD* tumor suppressor gene. We describe here the involvement of the AMPK–MAPO1–FLCN complex in the signaling pathway of apoptosis induced by O^6-methylguanine. By the introduction of siRNAs specific for these genes, the transition of cells to a population with sub-G_1 DNA content following MNU treatment was significantly suppressed. After MNU exposure, phosphorylation of AMPKα occurred in an MLH1-dependent manner, and this activation of AMPK was not observed in cells in which the expression of either the *Mapo1* or the *Flcn* gene was downregulated. When cells were treated with AICA-ribose (AICAR), a specific activator of AMPK, activation of AMPK was also observed in a MAPO1- and FLCN-dependent manner, thus leading to cell death which was accompanied by the depolarization of the mitochondrial membrane, a hallmark of the apoptosis induction. It is therefore likely that MAPO1, in its association with FLCN, may regulate the activation of AMPK to control the induction of apoptosis triggered by O^6-methylguanine.

1. Introduction

Most of the DNA lesions produced by internal and external agents can be removed by cellular DNA repair enzymes, while cells with un-repaired lesions are eliminated by apoptosis. The biological significance of these two mechanisms is clearly shown when organisms lacking one or both of these cellular functions are exposed to simple alkylating agents, such as *N*-methyl-*N*-nitrosourea (MNU) and *N*-methyl-*N'*-nitro-*N*-nitrosoguanidine (MNNG), which alkylate purine and pyrimidine bases in DNA [1]. Among the various modified bases thus produced, O^6-methylguanine is of particular importance since this modified base can pair with thymine as well as cytosine during DNA replication, leading to induction of mutation and cancer [2,3]. Organisms possess a specific DNA repair enzyme, O^6-methylguanine–DNA methyltransferase (MGMT), which transfers a methyl-group from O^6-methylguanine in DNA onto the enzyme molecule, thereby repairing the DNA lesion in a single step reaction [4,5]. When the modified base is not repaired, an O^6-methylguanine–thymine pair is formed through DNA replication and this mismatch can be recognized by a mismatch repair protein complex, composed of MSH2, MSH6, MLH1 and PMS2, which induces apoptosis to exclude cells carrying the mutation-evoking DNA lesions [6–8]. It is noteworthy that *Mgmt*$^{-/-}$ mice, which lack the DNA repair enzyme specific for O^6-methylguanine, are hypersensitive to both the killing and to the tumorigenic action of alkylating chemicals [9–12] and these dual effects can be dissociated by the introduction of an additional defect in mismatch repair genes. Mice with mutations in both alleles of the *Mgmt* and the *Mlh1* genes, the latter encoding a protein involved in the recognition of mismatched base, are as resistant to MNU as are wild-type mice in terms of survival, but are much more susceptible to MNU-induced tumorigenesis than wild-type mice

* Corresponding author at: Department of Physiological Science and Molecular Biology, Fukuoka Dental College, 2-15-1 Tamura, Sawara-ku, Fukuoka 814-0193, Japan. Tel.: +81 92 801 0411x310; fax: +81 92 801 0685.
E-mail address: hidaka@college.fdcnet.ac.jp (M. Hidaka).

1568-7864/$ – see front matter © 2011 Elsevier B.V. All rights reserved.
doi:10.1016/j.dnarep.2011.11.006

[13]. Consistent with these results, *Mgmt*$^{-/-}$ *Mlh1*$^{-/-}$ cells, derived from the gene-targeted mice, are unable to induce apoptosis and show an elevated mutant frequency after MNU treatment [14].

The apoptotic signal initiated through the mismatch recognition complex activates a signaling cascade leading to the cell cycle checkpoints and apoptotic pathways for cell death. Both the release of cytochrome C from the mitochondria as well as the activation of Apaf-1 and caspase-3, hallmarks of the induction of apoptosis, have been demonstrated after the treatment of cells with alkylating agents that produce O^6-methylguanine [14,15]. However, the precise molecular mechanism underlying the signal transduction downstream of mismatch recognition still remains to be determined. To identify the factors involved in the O^6-methylguanine-induced apoptotic process, we screened MNU-resistant clones derived from MNU-sensitive *Mgmt*$^{-/-}$ cells using retrovirus-mediated gene-trap mutagenesis [16]. Mouse-derived KH101 cells, carrying an insertional mutation in one of the alleles of an uncharacterized gene, were unable to induce mitochondrial membrane depolarization as well as caspase-3 activation, after treatment with MNU. In this way, we identified a new gene, designated as *Mapo1* (O^6-methylguanine induced apoptosis 1), which was related to the induction of apoptosis. The mutant frequency of KH101 cells was significantly elevated after the treatment with MNU, thus supporting the notion that the induction of apoptosis, in which the MAPO1 is involved, contributes significantly to the elimination of cells carrying mutation-inducing DNA lesions. A search in the database revealed that the amino acid sequence of the MAPO1 protein is homologous to that of folliculin-interacting protein 1 (FNIP1), which was identified as a protein having the capacity to associate with folliculin [17]. Folliculin is a tumor suppressor protein with unknown biological activity, and is encoded by the *FLCN* gene. Mutations in the *FLCN* gene have been found in patients with Birt-Hogg-Dubé (BHD) syndrome [18,19], which is characterized by the development of hair follicle hamartomas, lung cysts, and an increased risk for renal neoplasia [20–22]. Identification of another folliculin-interacting protein, displaying a similarity in its amino acid sequence to that of FNIP1, was reported by two groups of researchers and the gene responsible was named *FNIP2* and *FNIPL*, respectively [23,24]. The *FNIP2/FNIPL* gene turned out to be the same gene as the human homolog of *Mapo1*. It was also reported that FNIP2/FNIPL, as well as FNIP1, could bind to 5′-AMP-activated protein kinase (AMPK), composed of AMPKα, β and γ subunits, which is an important energy sensor in cells that negatively regulates cell growth and proliferation [25,26].

We report here that a complex composed of MAPO1, FLCN and AMPK is involved in the induction of apoptosis triggered by O^6-methylguanine–thymine mispair. Evidence is presented which shows that during the course of apoptosis induction, the phosphorylation of AMPKα occurs in a MAPO1- and FLCN-dependent manner.

2. Materials and methods

2.1. Cell lines and cell culture

The YT102 (*Mgmt*$^{-/-}$ *Mlh1*$^{+/+}$), YT103 (*Mgmt*$^{-/-}$ *Mlh1*$^{-/-}$) and KH101 (*Mgmt*$^{-/-}$ *Mapo1*$^{+/-}$) cell lines were established as described previously [14,16]. The cells were cultivated in Dulbecco's modified Eagle's medium (D-MEM) supplemented with 10% fetal bovine serum (FBS) at 37 °C in 5% CO_2.

2.2. Chemicals

N-Methyl-*N*-nitrosourea (MNU) was obtained from Sigma. Compound C and AICA-Ribose were purchased from Calbiochem.

2.3. Immunoprecipitation and immunoblotting

To prepare cells expressing Flag-tagged MAPO1 or HA-tagged FLCN, a pIRES-puro3 vector (Clontech) containing mouse-derived *Mapo1* cDNA tagged with Flag epitope at the carboxy terminal end or a pIRES-puro2 (Clontech) vector carrying mouse-derived *Flcn* cDNA tagged with the HA epitope at the amino terminal end was introduced into YT102 cells using Lipofectamine 2000 (Invitrogen) according to the manufacturer's protocol. For the immunoprecipitation, the cells were lysed with NETN buffer (50 mM Tris/HCl (pH 8.0), 150 mM NaCl, 0.2% NP-40, 1 mM EDTA) containing protease inhibitors (Roche). To precipitate the Flag-tagged MAPO1, 10 μl of anti-FLAG M2-agarose (Sigma) were added to the extract, and incubated for 4 h at 4 °C. Alternatively, 10 μl of anti-HA (HA-7)-agarose (Sigma) were added to precipitate the HA-tagged FLCN, and the mixture was incubated overnight at 4 °C. After extensive washing of the beads with NETN buffer, the proteins bound to the beads were eluted in 40 μl of 2× SDS-PAGE sample buffer (120 mM Tris/HCl (pH 6.8), 4% SDS, 20% glycerol, 200 mM DTT, 0.002% bromophenol blue).

For the immunoblotting analyses, immunoprecipitated materials or whole cell extracts prepared by the lysis of cells with 2× SDS-PAGE sample buffer were subjected to SDS-PAGE and electroblotted onto a PVDF membrane (Bio-Rad). Detection was performed using an ECL Plus or Advance Western blotting detection kit (GE Healthcare). The primary antibodies used were: anti-FLAG M2 (Sigma), anti-HA HA-7 (Sigma), anti-FLCN (Protein Tech Group, Inc.), anti-AMPKα (Cell signaling), anti-β-actin (Sigma), and anti-phospho-AMPKα (Thr172) (Cell signaling). Anti-mouse IgG and anti-rabbit IgG conjugated to horseradish peroxidase (GE Healthcare) were used as the secondary antibodies.

2.4. siRNA transfection

Stealth RNAi for the *Mapo1* gene (siMapo1), 5′-CAGAAAGCAGAGGAUGUUCCUAUUA-3′, *Flcn* gene (siFlcn#1), 5′-UUAUUCAGGAUAGUGGGCCCAACUC-3′, (siFlcn#2), 5′-UGGUGACUGACGUACUUAAUAGAGG-3′, and *Ampkα* gene (siAmpkα#1), 5′-UAUCUUAGCGUUCAUCUGGGCAUCC-3′, (siAmpkα#2), 5′-AAGAUGAUAAGCCACUGCAAGCUGG-3′ were purchased from Invitrogen. After culturing 1×10^5 cells in a 6-well plate for one day, the cells were transfected with 20 nM siRNA, using the Lipofectamine RNAiMAX reagent (Invitrogen) according to the manufacturer's protocol. For the control transfection, Stealth RNAi Negative Control Medium GC Duplex (Invitrogen) was used.

2.5. Flow cytometric analysis

For the sub-G_1 population assay, cells were washed with PBS and suspended in 400 μl of PBS containing 0.1% Triton X-100, 25 μg/ml of propidium iodide and 0.1 mg/ml of RNase A. The samples were analyzed using a FACS Calibur flow cytometer (Becton Dickinson), with 10,000 events per determination.

For the mitochondrial membrane depolarization assay, cells were treated with the MitoProbeTM DiOC2(3) Assay Kit (Invitrogen), according to the manufacturer's protocol, and then subjected to analysis using a FACS Calibur flow cytometer.

2.6. Trypan blue exclusion assay

The viability of YT102, KH101 and siRNA-transfected YT102 cells was assayed, based on their trypan blue exclusion. The cells treated with AICA-Ribose were collected 48 h after the drug treatment and were stained with 0.2% trypan blue. The percentage of dead cells was determined as the percentage of trypan blue staining-positive cells. At least 500 cells were counted per experiment.

2.7. Statistics

All *P*-values were generated using two-tailed Student's *t*-tests.

3. Results

3.1. Interaction of MAPO1 with FLCN and AMPK

To confirm that MAPO1 protein interacts with FLCN and AMPK, a co-immunoprecipitation experiment was performed. Whole cell extracts were prepared from mouse YT102 (*Mgmt*$^{-/-}$) cells expressing Flag-tagged MAPO1, and were subjected to immunoprecipitation using an anti-Flag antibody conjugated to agarose beads. The results are shown in Fig. 1A. With whole cell extracts, almost the same intensity of bands for FLCN and AMPKα were detected in both control and Flag-MAPO1-transfected cells. When the materials were immunoprecipitated with the anti-Flag antibody, co-precipitated FLCN and AMPKα were clearly detected, concomitant with the effective precipitation of Flag-MAPO1, whereas no such bands were seen in a sample precipitated from cells treated with the control vector alone.

To evaluate the interaction of FLCN with MAPO1 and AMPK in a reciprocal manner, whole cell extracts prepared from YT102 cells expressing FLAG-tagged MAPO1, with or without HA-tagged FLCN, were applied for immunoprecipitation using an anti-HA antibody (Fig. 1B). When the HA-tagged FLCN was precipitated, as indicated by doublet bands by the immunoblotting analysis, the Flag-tagged MAPO1 and AMPKα were co-precipitated. It is evident, therefore, that MAPO1 interacts with FLCN and AMPK in mouse cells.

3.2. Suppression of the induction of apoptosis in Flcn- and Ampkα-knockdown cells

Since MAPO1 has been identified as an apoptosis-inducing protein, it is plausible that the MAPO1-bound proteins, FLCN and AMPK, might also be involved in apoptosis induction. To examine the possible roles of these proteins, siRNAs specific for the *Flcn* or *Ampkα* genes were introduced into YT102 (*Mgmt*$^{-/-}$) cells. As shown in Fig. 2A and B, two independent siRNAs (siFlcn#1 and #2, and siAmpkα#1 and #2), designed at different sequences of each gene, effectively suppressed the expression of the genes when measured at 48 h after their introduction. The expression level of the *Mapo1* gene in siMapo1-treated cells also decreased to 43% of that in cells that were treated with the control RNA, siCont, as measured by quantitative real time PCR [16]. To monitor the appearance of cells with sub-G_1 DNA content, cells were treated with or without 0.4 mM MNU for 1 h and subjected to a flow cytometric analysis 72 h later. After treatment with MNU, the sub-G_1 cell population increased to more than 20% in the siCont-treated cells (Fig. 2C). Under the same conditions, the degrees of the increases in the cells treated with siRNAs against the *Flcn*, *Ampkα* and *Mapo1* genes were significantly suppressed. These results favor the notion that FLCN and AMPKα, as well as MAPO1, are involved in MNU-induced apoptosis through protein interactions.

3.3. Suppression of the induction of apoptosis by an AMPK inhibitor

The effects of *Ampkα* knockdown on the MNU-induced apoptosis were further examined at multiple time points. The YT102 cells transfected with siCont or siAmpkα#2 were exposed to 0.4 mM MNU for 1 h and then subjected to a flow cytmetric analysis. As shown in Fig. 3A, the sub-G_1 cell population increased gradually, with similar kinetics in cells transfected with either type of siRNA, but the degree of the increase in cells transfected with siAmpkα was significantly lower than that of siCont-transfected cells.

To obtain further evidence supporting the involvement of AMPK in MNU-induced apoptosis, compound C, a specific inhibitor of AMPK, was used to downregulate the function of AMPK. YT102 cells were exposed to 0.4 mM MNU for 1 h, followed by incubation with or without 2 μM of compound C for 72 h, and then cells were subjected to a flow cytometric analysis. As shown in Fig. 3B, the sub-G_1 cell population in compound C-treated cells after MNU treatment significantly decreased in comparison to those not treated with the inhibitor. The inhibitory effects of compound C on AMPK activity were assessed by immunoblotting using an antibody that specifically recognizes a phosphorylated form of AMPKα, since AMPK is activated when the catalytic subunit of AMPKα becomes phosphorylated [27–29]. As shown in Fig. 3C, AMPK appeared to be activated after MNU treatment, while such activation was significantly suppressed by the exposure of cells to compound C. These findings are consistent with the notion that AMPK plays an important role in the induction of apoptosis triggered by MNU.

3.4. MAPO1- and FLCN-dependent activation of AMPK during the induction of apoptosis

To further examine if AMPKα is phosphorylated during the induction of apoptosis, YT102 cells were treated with 1 mM MNU and then collected at 0, 24, 48 and 72 h after treatment. Under these conditions, apoptosis was effectively induced, as was evident by the detection of the mitochondrial membrane depolarization and the caspase-3 activity [16]. The whole cell extracts were prepared, and the phosphorylation levels of AMPKα were assessed by

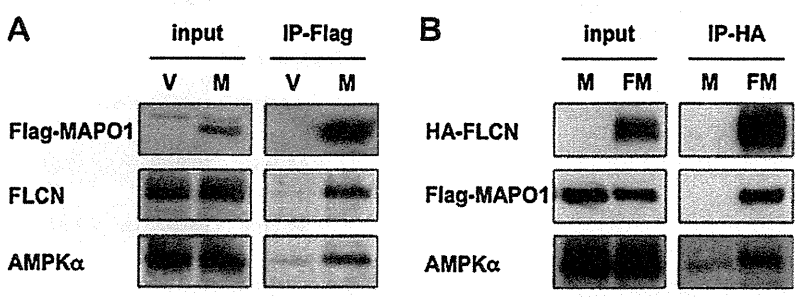

Fig. 1. The association of MAPO1, FLCN and AMPKα proteins. (A) The interaction of MAPO1 with FLCN and AMPKα. YT102 cells were transfected with the pIRES-puro3 vector (termed as V) or pIRES-puro3 containing Flag-tagged *Mapo1* cDNA (termed as M) and harvested after incubation for 24 h. Whole cell extracts (input) were used for immunoprecipitation using anti-Flag M2 antibody beads (IP-Flag). The materials were subjected to SDS-PAGE, transferred to a membrane and immunoblotted using antibodies that recognize the Flag-tag, FLCN and AMPKα. (B) The interaction of FLCN with MAPO1 and AMPKα. YT102 cells were transfected with either pIRES-puro3 containing Flag-tagged *Mapo1* cDNA (termed as M) or pIRE-puro2 carrying HA-tagged *Flcn* cDNA and pIRES-puro3 containing Flag-tagged *Mapo1* cDNA (termed as FM) and were harvested 24 h later. Following immunoprecipitation using anti-HA HA7 antibody beads (IP-HA), an immunoblotting analysis was performed as described in (A) with anti-HA, anti-Flag and anti-AMPKα antibodies.

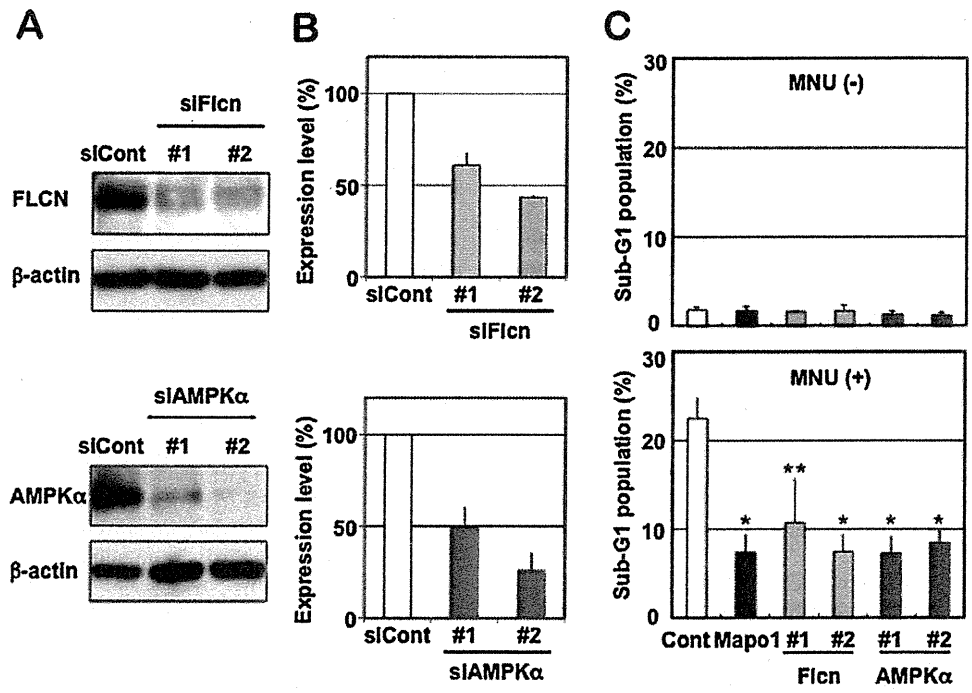

Fig. 2. The suppression of apoptosis by siRNAs targeting the three types of genes. (A) The expression levels of FLCN and AMPKα in cells treated with siRNAs. The whole extracts of YT102 cells transfected with control and two independent siRNAs specific for the corresponding genes were used for the immunoblotting analysis with antibodies specific for FLCN, AMPKα and β-actin (loading control). (B) The relative expression levels of FLCN and AMPKα in the cells treated with siRNAs, as measured by an immunoblotting analysis in (A). (C) The sub-G_1 population of cells transfected with control, *Mapo1*-, *Flcn*- or *Ampkα*-siRNA after MNU treatment. Two days after transfection with siRNA, YT102 cells were treated with or without 0.4 mM MNU for 1 h and then incubated for three days. The cells were harvested and subjected to a flow cytometric analysis. $^*P < 0.01$; $^{**}P < 0.05$ when comparing the sub-G_1 populations in the control and gene-specific siRNA-transfected cells.

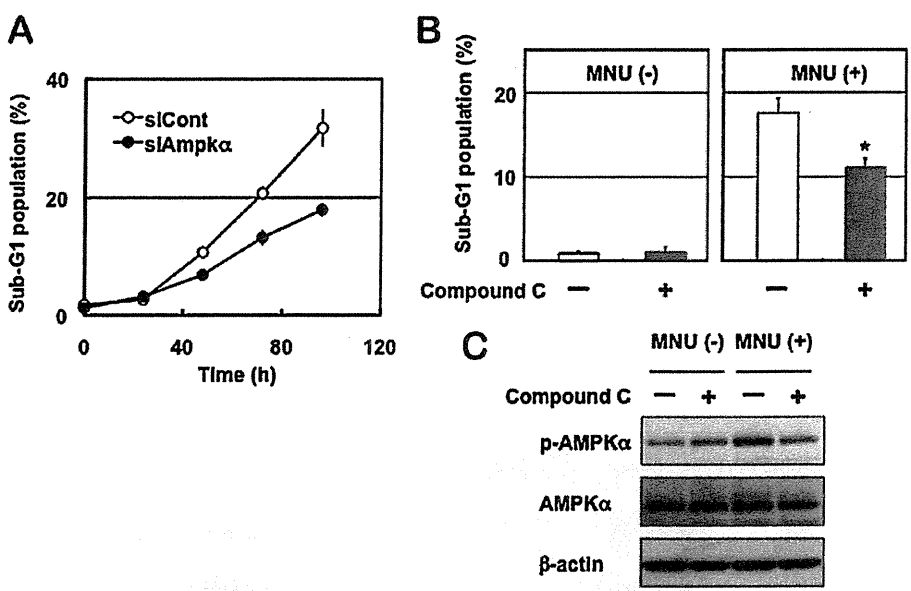

Fig. 3. The involvement of AMPK in MNU-induced apoptosis. (A) The sub-G_1 population of cells transfected with control or *Ampkα* siRNA after MNU treatment. Two days after transfection with siRNA, the YT102 cells were treated with 0.4 mM MNU for 1 h and then harvested at 0, 24, 48, 72 and 96 h after MNU treatment, and subjected to a flow cytometric analysis. The numbers of the cells in the sub-G_1 population were counted and the ratios were plotted. Open circles, siCont-transfected cells; closed circles, siAmpkα-transfected cells. (B) The suppression of apoptosis by an AMPK inhibitor. After treatment with or without 0.4 mM MNU for 1 h, YT102 cells were incubated in medium supplemented with or without 2 μM compound C for three days. The cells were then harvested and subjected to a flow cytometric analysis to monitor the sub-G_1 population of cells. $^*P < 0.01$ when comparing the sub-G_1 populations in compound C-untreated and compound C-treated cells after exposure to MNU. (C) The inhibition of the AMPK activity by compound C. The whole cell extracts from the cells harvested at 48 h after MNU treatment were subjected to an immunoblotting analysis using antibodies that recognize phospho-AMPKα (Thr172), AMPKα and β-actin, respectively.

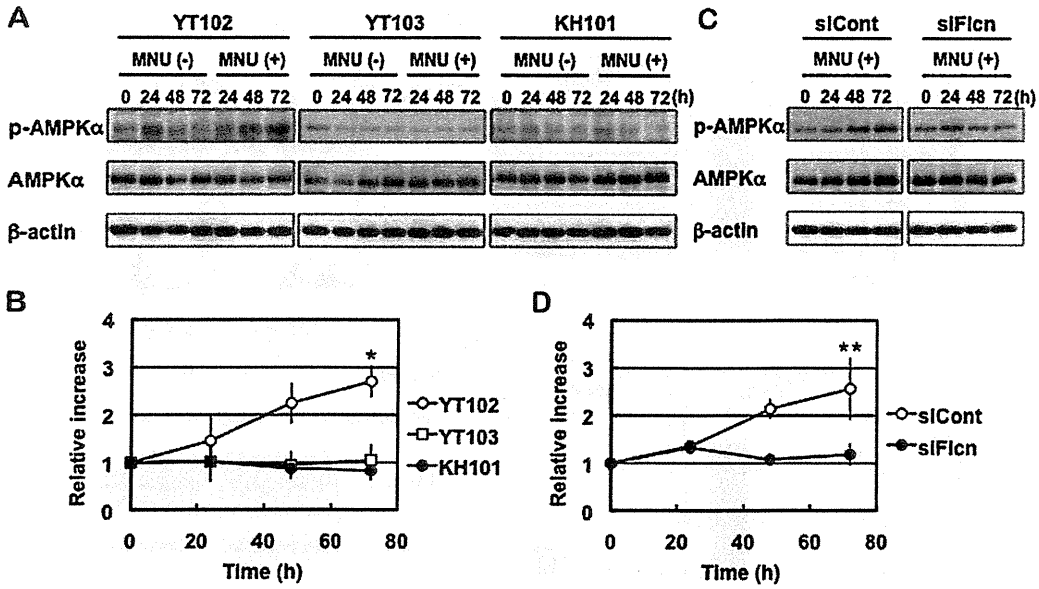

Fig. 4. The activation of AMPK after MNU treatment. (A) The phosphorylation of AMPKα in cells with different genetic backgrounds. Three cell lines, YT102 (*Mgmt*$^{-/-}$), YT103 (*Mgmt*$^{-/-}$ *Mlh1*$^{-/-}$) and KH101 (*Mgmt*$^{-/-}$ *Mapo1*$^{+/-}$), were treated with or without 1 mM MNU for 1 h and then incubated for 0, 24, 48 or 72 h. The whole cell extracts from cells harvested at various times after MNU treatment were subjected to an immunoblotting analysis using antibodies that recognize phospho-AMPKα (Thr172), AMPKα and β-actin, respectively. (B) The relative intensities of the bands for phospho-AMPKα (Thr172) after MNU treatment. Open circles, YT102; open squares, YT103; closed circles, KH101. *$P < 0.01$ when comparing the relative intensities for YT102 cells with those of the YT103 and KH101 cells at 72 h after exposure to MNU. (C) Activation of AMPK in cells transfected with *Flcn*-siRNA. Two days after transfection with control or *Flcn*-siRNA, the YT102 cells were treated with or without 1 mM MNU for 1 h. The analysis was performed as described above. (D) The relative intensities of bands for phospho-AMPKα (Thr172) after MNU treatment. Open circles, siCont-transfected cells; closed circles, siFlcn-transfected cells. **$P < 0.05$ when comparing the relative intensities of the control and *Flcn*-specific siRNA-transfected cells at 72 h after exposure to MNU.

an immunoblotting analysis. As shown in Fig. 4A and B, the levels of phosphorylation of AMPKα increased gradually and reached about 2.7-folds at 72 h after MNU treatment, whereas no such increase was observed in cells not expose to MNU. The amounts of the AMPKα protein were almost constant under these situations. In YT103 (*Mgmt*$^{-/-}$ *Mlh1*$^{-/-}$) cells, which are unable to induce apoptosis due to their lack of the *Mlh1* gene, the increase of phosphorylated forms of AMPKα was hardly detectable, even after MNU treatment. These results indicate that AMPK is activated during the course of the induction of apoptosis, triggered in a mismatch repair protein-dependent manner. To evaluate the effects of *Mapo1* mutation on the activation of AMPK, we used KH101 (*Mgmt*$^{-/-}$ *Mapo1*$^{+/-}$) cells, which carry an insertional mutation in one of the alleles of the *Mapo1* gene and exhibit haploinsufficiency for the induction of apoptosis triggered by MNU treatment [16]. Similar to the results described above, no increase in the band corresponding to phosphorylated AMPKα was detected even after treatment with MNU (Fig. 4A and B). Since MAPO1 interacts with FLCN (Fig. 1), it was supposed that FLCN might also play a role in the activation of AMPK during the course of apoptosis. To examine this possibility, YT102 (*Mgmt*$^{-/-}$) cells were transfected with siRNA targeting the *Flcn* gene (siFlcn#2), and then were exposed to 1 mM MNU for 1 h. The immunoblotting analyses of these samples collected after incubation for 0, 24, 48 and 72 h revealed that phosphorylation of AMPKα, which occurred gradually in siCont-transfected cells, did not take place in the siFlcn-transfected ones (Fig. 4C and D). These results indicate that the activation of AMPK, which occurs during the course of MNU-induced apoptosis, is dependent on the functions of both FLCN and MAPO1.

3.5. Induction of apoptosis through activation of AMPK

To confirm the importance of the activation of AMPK for the induction of apoptosis, AICA-Ribose (AICAR), a specific activator of AMPK, was applied to YT102 cells. After treatment with a low dose (0.2 mM) of AICAR for 48 h, the viabilities of cells were analyzed, based on the trypan blue exclusion assay. As shown in Fig. 5A, there was a significant increase of trypan blue staining-positive cells after treatment with AICAR in the YT102 (*Mgmt*$^{-/-}$ *Mapo1*$^{+/+}$) cells, whereas no such increase was observed in the *Mapo1*-defective KH101 (*Mgmt*$^{-/-}$ *Mapo1*$^{+/-}$) cells even after the same treatment. To determine if the increase in dead cells was related to the induction of apoptosis, the cells were subjected to an assay for mitochondrial membrane depolarization, which is known to occur during the process of apoptosis. The results are shown in Fig. 5B and C. The depolarization of the mitochondrial membrane was induced after treatment with AICAR in YT102 cells, but not in *Mapo1*-defective KH101 cells. The results indicate that the function of MAPO1 is necessary for AICAR-induced apoptosis. An immunoblotting experiment, the results of which are shown in Fig. 5D, revealed that the AICAR-treatment induced phosphorylation of AMPKα to the similar level to that when treated with MNU, however, such an induction did not occur in the *Mapo1*-defective KH101 cells. These results suggest that the activation of AMPK is important for the induction of apoptosis, and that a normal level of MAPO1 is necessary for the activation of AMPK.

We next examined if FLCN, which interacts with MAPO1, is also required for the AICAR-induced cell death. For this study, we applied AICAR to YT102 cells whose FLCN function was knocked down by siRNA (siFlcn#2). As shown in Fig. 6A–C, the degree of AICAR-induced cell death, which was accompanied by the depolarization of the mitochondrial membrane, was significantly lower in siFlcn-transfected cells as compared to that in siCont-transfected ones. Furthermore, the AICAR-induced AMPKα phosphorylation was almost completely blocked in siFlcn-transfected cells (Fig. 6D). Therefore, these results suggest that FLCN is required for AMPK activation, as well as the cell death induced by the treatment with AICAR.

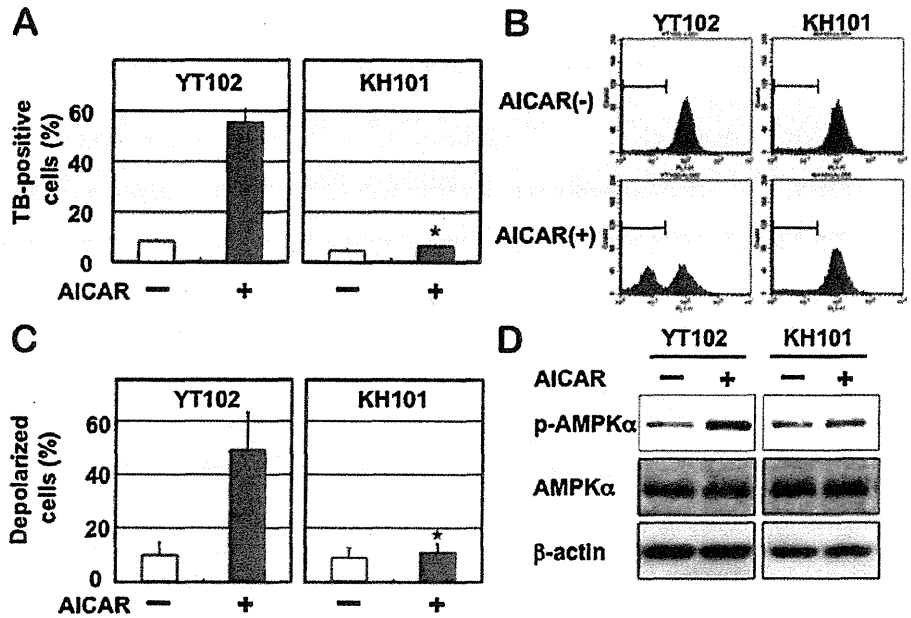

Fig. 5. MAPO1-dependent cell death induced by an AMPK activator. *Mapo1*-proficient YT102 and *Mapo1*-defective KH101 cells were incubated in a medium supplemented with or without 0.2 mM AICAR for two days and then harvested. (A) The viabilities of the cells. The numbers of cells stained with trypan blue (TB) were counted and the ratios are shown. *$P < 0.01$ when comparing the TB-positive YT102 and KH101 cells after exposure to AICAR. (B) Depolarization of the mitochondrial membrane. The cells were evaluated by a mitochondrial membrane depolarization assay, and representative patterns of the assay are shown. The populations of depolarized cells were gated by bars. (C) The levels of mitochondrial membrane depolarization. The mean values obtained from three independent experiments in (B) and the standard deviations (bars) are presented. *$P < 0.01$ when comparing the depolarized cells in YT102 and KH101 cells after exposure to AICAR. (D) Activation of AMPK after treatment with AICAR. The whole cell extracts prepared from cells, treated with or without AICAR, were subjected to an immunoblotting analysis using antibodies specific for phospho-AMPKα (Thr172), AMPKα and β-actin, respectively.

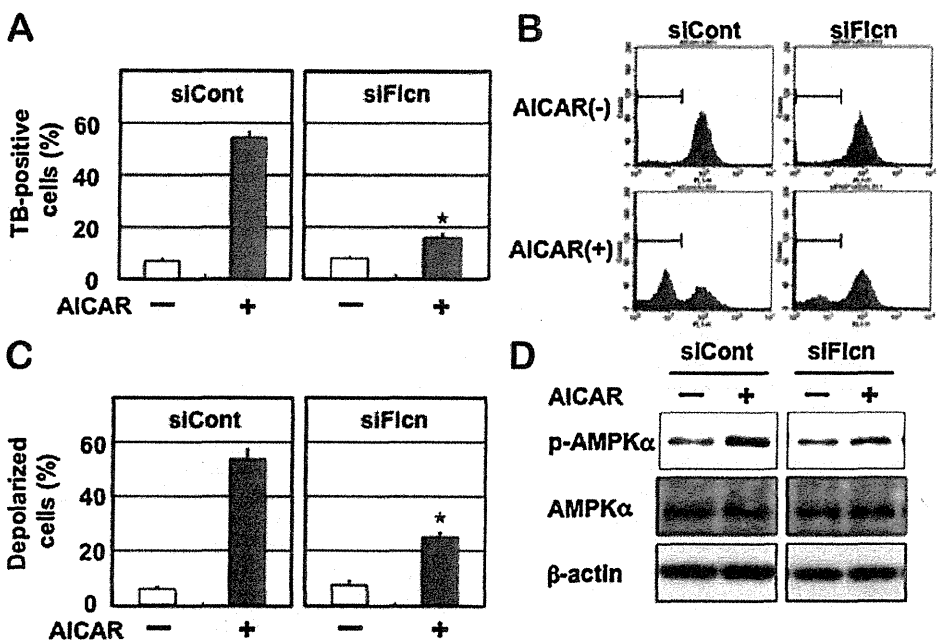

Fig. 6. FLCN-dependent cell death induced by an AMPK activator. YT102 cells transfected with control- or *Flcn*-siRNA were cultured with or without 0.2 mM AICAR for two days and then harvested. (A) The viabilities of the cells. The numbers of cells stained with trypan blue (TB) were counted and the ratios are shown. *$P < 0.01$ when comparing the TB-positive siCont-transfected and siFlcn-transfected cells after exposure to AICAR. (B) Depolarization of the mitochondrial membrane. The cells were evaluated by a mitochondrial membrane depolarization assay, and representative patterns of the assay are shown. The populations of depolarized cells were gated by bars. (C) The levels of mitochondrial membrane depolarization. The mean values obtained from three independent experiments in (B) and the standard deviations (bars) are presented. *$P < 0.01$ when comparing the depolarized cells in siCont-transfected and siFlcn-transfected cells after exposure to AICAR. (D) Activation of AMPK after treatment with AICAR. The whole cell extracts prepared from AICAR-treated or -untreated cells, were subjected to an immunoblotting analysis using antibodies specific for phospho-AMPKα (Thr172), AMPKα and β-actin, respectively.